Title

Retinal bipolar cells borrow excitability from amacrine cells to amplify spatial features in dim light

Author List

Shubhash Chandra Yadav[1], Logan Ganzen[1], Lawrence Man[1], Hong Ma[1], Scott Nawy[1], Richard H Kramer[1]

1. University of California Berkeley, Department of Neuroscience. Berkeley, CA, USA.

Abstract

Bipolar cells (BCs) carry visual information from photoreceptors in the outer retina to retinal ganglion cells (RGCs) in the inner retina. Most BCs lack voltage-gated Na^+ (NaV) channels and action potentials. Instead, voltage signals spread passively from input to output synapses. Despite this, we find that blocking NaV channels reduces synaptic output of On-cone bipolar cells (On-CBCs). These cells borrow NaV channel-mediated excitability from electrically coupled A2 amacrine cells to amplify excitatory output, allowing voltage changes to be transmitted more effectively to downstream RGCs in dim light. Because neighboring On-CBCs form electrical synapses onto the same A2 cell, a spatially adjacent group of On-CBCs is more effective than a dispersed set for recruiting A2 cell electrical excitability and driving post-synaptic RGCs. This mechanism filters the neural representation of an image to highlight shapes over spatially uncorrelated stimuli, a sophisticated feature detection property that is well-suited for object recognition.

Author approvals

All authors have seen and approved the manuscript. The manuscript has not been submitted or published elsewhere.

Competing interests

The authors declare no competing interests.

Acknowledgements

We are grateful to Karin Dedek for helping us with retinal imaging, Denis Delkara and Olivier Marre for useful suggestions about marker gene targeting, and Mei Li for manufacturing AAV vectors. We would like to especially thank Gregory Schwartz for carefully reading our manuscript and for his helpful comments. This project was funded by NIH grants P30EY003176 and R01EY024334 to Richard H Kramer.

Author contributions

Yadav SC, Nawy S and Kramer RH conceptualized the project; Yadav SC and Kramer RH designed the experiments; Yadav SC performed the electrophysiology experiments with help from Ganzen L and Nawy S; Man L helped with the acquisition of images; Ma H helped with the generation of cre-mice and gene editing; Yadav SC and Nawy S analyzed the data; Yadav SC and Kramer RH wrote the paper; Kramer RH supervised the project.

40 **INTRODUCTION**

41 Neurons in the brain use propagating action potentials to send signals over long
42 distances. In contrast, many retinal neurons, including rod and cone photoreceptors,
43 horizontal cells, and bipolar cells (BCs), are so short that action potentials are
44 unnecessary. In BCs, graded voltage signals generated at input synapses in the outer
45 retina spread passively to output synapses in the inner retina, eliciting graded
46 neurotransmitter release. Consistent with the lack of action potentials, most
47 mammalian BCs lack voltage-gated Na^+ (NaV) channels[1-7], and in the few BCs types
48 where NaV channels are found, expression is insufficient to support spiking[8,9].

49 Retinal ganglion cells (RGCs) and amacrine cells are the only classes of retinal
50 neurons that do generate NaV-dependent action potentials. RGCs have axons that
51 extend centimeters through the optic nerve to visual centers in the brain and NaV
52 channels are needed for initiating and propagating spikes along these axons. Wide-
53 field amacrine cells (wf-ACs) have long lateral processes projecting up to 2 mm, and
54 in many wf-Acs, NaV channels support the propagation of dendritic spikes over these
55 long distances[10]. Some medium-field amacrine cells (mf-ACs, typically 150-500 μm)
56 are also excitable, including starburst amacrine cells that respond preferentially to
57 visual stimuli moving in a particular direction[11]. But while dendritic excitability enhances
58 directional selectivity of starburst cells[12,13], it is not necessary for its occurrence[14].

59 While many narrow field amacrine cells are inexcitable, some, such as the axon-less
60 A2 amacrine cell, have abundant NaV channels, even though their dendritic processes
61 extend only 30-40 μm. Rather than residing along dendrites, NaV channels in A2 cells
62 cluster in a thin, unbranched appendage, devoid of synapses but rich in expression of
63 ankyrin G, a NaV scaffolding protein normally found in the axon initial segment (AIS)
64 of axon-containing neurons[15]. The role of NaV channels in A2 amacrine cells and the
65 significance of this appendage, which is an electrotonic dead end, has remained a
66 mystery.

67 In addition to long distance signaling, NaV-mediated excitability serves other functions.
68 Because action potentials exhibit a threshold, NaV-mediated excitability can make
69 dendritic integration of synaptic inputs a highly non-linear process, as has been
70 observed in some wf-ACs[16]. Because action potentials are typically all-or none, NaV-
71 mediated excitability can standardize depolarizing voltage changes, increasing the
72 reliability of synaptic output. The rapid rate of rise of depolarization mediated by

regenerative activation of NaV channels can accelerate synaptic output, as has been observed at the A2 output synapses[17].

Our knowledge of AC function comes mostly from experiments utilizing natural light stimuli to activate rod and/or cone pathways. However, there are 15 types of BCs [18,19] and >60 types of ACs in the mouse retina, many of which converge onto common sets of RGCs[20]. This makes it difficult to evaluate the role of individual BC and AC types in determining RGC light responses and nearly impossible to understand how electrical excitability contributes. To simplify analysis, we targeted expression of an optogenetic tool to one specific type of On-CBC; the type 6 cone bipolar cell (CBC6), which forms an electrical synapse predominantly with one type of AC; the A2 amacrine cell[21]. In turn, the CBC6 cell makes a chemical excitatory synapse on the On-alpha RGC[22], a ganglion cell type which plays a key role in processing both rod-mediated[23] and cone-driven signals[24].

Studying this circuit in isolation is a challenge, but by pharmacologically blocking all inhibitory and excitatory chemical synaptic inputs onto CBC6 and A2 cells with neurotransmitter receptor inhibitors while sparing only the AMPA receptors on RGCs, we could selectively examine the effect of A2 cells on CBC6 cell output. Once we understood the role of NaV-mediated excitability in this isolated circuit, we could then evaluate its role in the intact retinal circuit responding naturally to cone-driven light stimuli. Using this strategy, we found that NaV-mediated excitability of A2 amacrine cells amplifies synaptic output of On-CBCs, but only to spatially clustered stimuli, providing a neural mechanism for distinguishing objects over spatially distributed background, early in the visual system.

RESULTS

Investigating voltage-gated Na^+ channels and intrinsic excitability of On-CBCs and A2 amacrine cells

To investigate the possible presence of voltage-gated Na^+ channels in On-CBCs and A2 amacrine cells, we recorded voltage-gated ionic currents from these cell types under whole-cell patch clamp. To isolate voltage-gated currents explicitly from the recorded cells, the retinas were pre-treated with 100 μM meclofenamic acid (MFA), an uncoupler of gap junctions[25]. First, we investigated CBC6 cells in the whole-mount mouse retinas. To identify and record from CBC6 cells, we utilized a cre-driver mouse

105 line, enabling transgene expression of a fluorescent protein marker, eYFP, in CBC6
106 cells, but no other types of BCs[26]. eYFP was fused to channelrhodopsin-2 (ChR2),
107 which we used for optogenetic manipulation in later experiments. The pipette solution
108 contained agents that blocked voltage-gated K^+ channels and the extracellular solution
109 had agents that blocked current through V-gated Ca^{2+} channels, allowing
110 measurement of NaV current in isolation.

111 In CBC6 cells, depolarizing voltage steps from a holding potential of -70 mV to 0 mV
112 elicited almost no inward current and bath application of the NaV channel blocker
113 tetrodotoxin (TTX) had no effect (Fig. 1a), consistent with a previous study suggesting
114 that NaV channels are absent from CBC6 cells[6]. We next obtained retinal slices and
115 recorded from A2 amacrine cells, which were tentatively identified by their size and
116 laminar location. The identity of putative A2 cells was verified by fluorescent dye-filling
117 to reveal their distinctive axodendritic morphology. In verified A2 cells, the depolarizing
118 voltage steps above -40 mV evoked a large inward current, which was blocked
119 completely by TTX (Fig. 1b) consistent with previous studies showing expression of
120 NaV channels and firing of action potentials[27,28]. Current-voltage curves substantiated
121 that while CBC6 cells lack NaV current, A2 amacrine cells have NaV current that can
122 be blocked with TTX (Extended Data Fig. 1a, b).

123 We next obtained cell-attached recordings on CBC6 cells or A2 cells in whole-mount
124 retinas to determine whether optogenetic stimulation can elicit action potentials in
125 either of these cells (Fig. 1c, e). To eliminate light responses transmitted from rod and
126 cone photoreceptors, synaptic transmission was blocked with agonist of mGluR6
127 receptors on On-BCs, and antagonist of kainate receptors on Off-BCs leaving ChR2 in
128 the CBC6 cell as the only relevant light sensor. A2 somata were targeted with the help
129 of mCherry expression (see Methods). Recordings from A2 somata showed consistent
130 all-or none transient spikes to each light flashes (Fig. 1d). TTX eliminated these events,
131 consistent with NaV-mediated action potentials. Recordings from CBC6 cell somata
132 showed no detectable spikes; however, recordings from presynaptic boutons of CBC6
133 cells revealed small spikes that were eliminated by adding TTX (Fig. 1f).

134 In addition to having an output synapse onto RGCs, CBC6 cells connect with A2
135 amacrine cells via gap junctions, localized on the CBC6 synaptic terminal in the On-
136 lamina of the inner plexiform layer (IPL)[29]. We hypothesized that the spikes detected

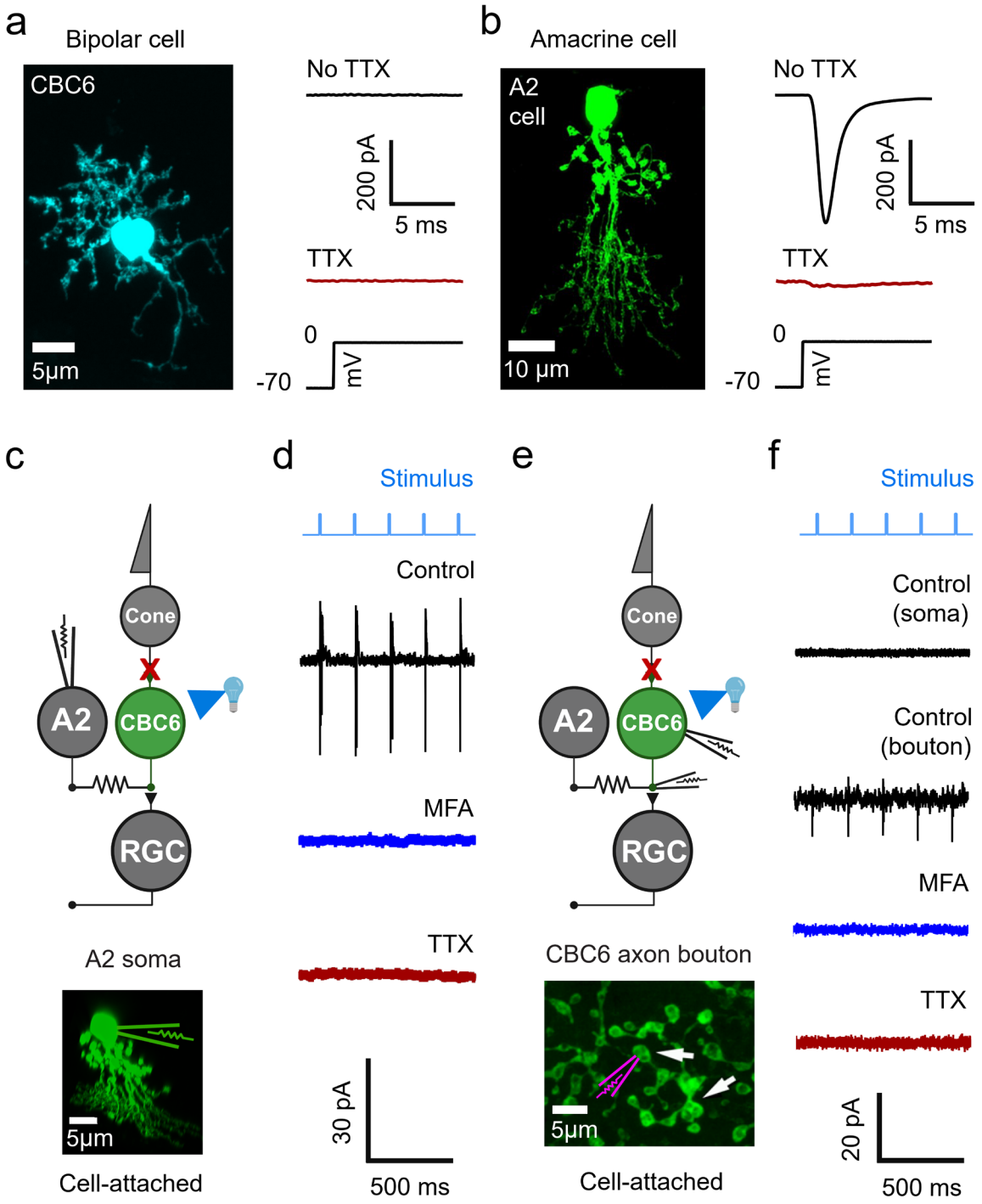

Figure 1. A2 amacrine cells exhibit NaV channel-mediated excitability but CBC6 bipolar cells do not. a, b) Intrinsic electrical properties of an A2 cell and an CBC6 cell, evaluated with the whole-cell patch clamp technique. Cells were filled with fluorescent dye (Alexa-594) and imaged with confocal microscopy to aid in visual identification. Under voltage-clamp, the A2 cell (b) exhibits depolarization-gated transient inward current that was blocked by TTX, characteristic of NaV channels, whereas the CBC6 cell (a) showed no inward current and no effect of TTX. **c-f)** Extracellular cell-attached patch recordings from A2 or CBC6 cells in a retina where

145 CBC6 cells express the optogenetic tool ChR2, as depicted in the retinal circuit
146 diagrams (green). Brief flashes of light (10 ms) elicited spikes in the soma of the A2
147 cell **(c-d)**, but not in the soma of the CBC6 cell **(e-f)**. However, recording from the CBC6
148 axon terminal did reveal small spikes. Spikes in both A2 somata and CBC6 terminals
149 were eliminated with TTX, implicating NaV channels. Spikes were also eliminated by
150 treatment with MFA, implicating gap junctions in transmitting the optogenetic
151 depolarization from the CBC6 terminal to the A2 cell and evoked spikes from the A2
152 cell back to the CBC6 terminals. See Extended Data Fig. 1.

153 in CBC6 cell terminals arose in the A2 cell and spread into the CBC6 cell through these
154 gap junctions. To test this, before recording we pre-treated whole-mount retinas for 45
155 minutes with MFA. Under these conditions, action potentials were absent from both
156 CBC6 cell terminals and A2 cells (Extended Data Fig. 1c, d). Together, these results
157 indicate that even though CBC6 cells do not possess their own NaV channels, their
158 voltage response is influenced by NaV channels in their electrically coupled partner,
159 the A2 amacrine cell.

160 **NaV channels amplify synaptic transmission from CBC6 cells.**

161 To evaluate chemical synaptic output from CBC6 cells, we stimulated the cells
162 optogenetically and measured responses in a postsynaptic On-alpha RGC (Fig. 2a).
163 Once again, synaptic inputs from rods and cones were blocked pharmacologically.
164 Brief flashes of light (2 ms) activated ChR2 in the CBC6 cells, depolarizing the
165 membrane potential enough to activate voltage-gated Ca^{2+} channels in their terminals,
166 leading to release of neurotransmitter onto RGCs[30]. Excitatory postsynaptic currents
167 (EPSCs) in RGCs reflect simultaneous stimulation of hundreds of CBC6 cells
168 converging onto an RGC, explaining its large amplitude (up to 3 nA). We found that
169 TTX reduced the peak amplitude of the EPSC by almost 70% (control=1894 ± 185 pA;
170 TTX=574 ± 99 pA; n=16 each; $p<0.0001$) (Fig. 2b, d). This indicates that synaptic
171 release from CBC6 is amplified by NaV channels, presumably in A2 amacrine cells
172 since the CBC6 cell have none of their own. TTX reduced the EPSCs across a wide
173 range of optogenetic stimulus strengths (Fig. 2h), indicating that NaV channels serve
174 to increase the gain of CBC6 cell to RGC synaptic transmission. TTX also increased
175 the rise time of the EPSC (control=9.8 ± 0.4 ms; TTX=13.4 ± 0.6 ms; n=16 each;

176 p<0.0001) and slowed its decay time (control=39.2 ± 4.7 ms; TTX=83.4 ± 12.1 ms;
177 n=16 each; p=0.0029) (Fig. 2b, e).

178 Strong or repeated depolarization of presynaptic neurons can lead to depletion of the
179 readily-releasable pool (RRP) of synaptic vesicles, resulting in synaptic depression[31].
180 We found that pairs of optogenetic stimuli, separated by an interval of 50 ms, leads to
181 paired-pulse depression of EPSCs recorded in RGCs, with the second being much
182 smaller than the first (Extended Data Fig. 2a). However, addition of TTX reduced
183 paired-pulse depression, usually replacing it with paired-pulse facilitation (Fig. 2c, f),
184 where the second stimulus elicits a larger response than the first (Extended Data Fig.
185 2b).

186 A possible explanation for all of these findings is that NaV channel-mediated excitability
187 of A2 cells amplifies and accelerates the depolarization of the CBC6 terminal, leading
188 to increased activation of voltage-gated Ca^{2+} channels, increased Ca^{2+} entry, and
189 enhanced Ca^{2+}-dependent fusion of synaptic vesicles, resulting in larger and faster
190 EPSCs[32]. If the amplification were sufficiently large to deplete the RRP, release elicited
191 by a second stimulus would be reduced, contributing to paired-pulse depression. In
192 addition, if the excitability of A2 cells exhibited refractoriness, perhaps because of NaV
193 inactivation, a second pulse might fail to generate an amplified response. Central to all
194 of these hypotheses is the role of gap junctions in enabling the initial depolarization to
195 spread from CBC6 cells to A2 cells and allowing the amplified response to spread back
196 into the CBC6 terminals.

197 To test the role of gap junctions in enabling amplification, we treated whole-mount
198 retinas with MFA. Under these conditions, when gap junctions were uncoupled, ESPCs
199 were unaffected by TTX (Fig. 2g). In fact, while TTX normally reduced CBC6 synaptic
200 transmission (Fig. 2h), TTX had no effect on EPSCs over a wide range of stimulus
201 strengths after MFA treatment (Fig. 2i). These findings are consistent with NaV-
202 mediated amplification arising from A2 cells, which MFA had removed from influencing
203 CBC6 cell synaptic release.

204 In addition to A2 amacrine cells, which have short dendritic projections and respond to
205 narrow-field illumination, the retina has many types of wf-ACs that also express NaV
206 channels[33]. Some wf-ACs receive direct or polysynaptic inputs from CBC6 cells and
207 they, in turn, synapse onto On-alpha RGCs[34,35].

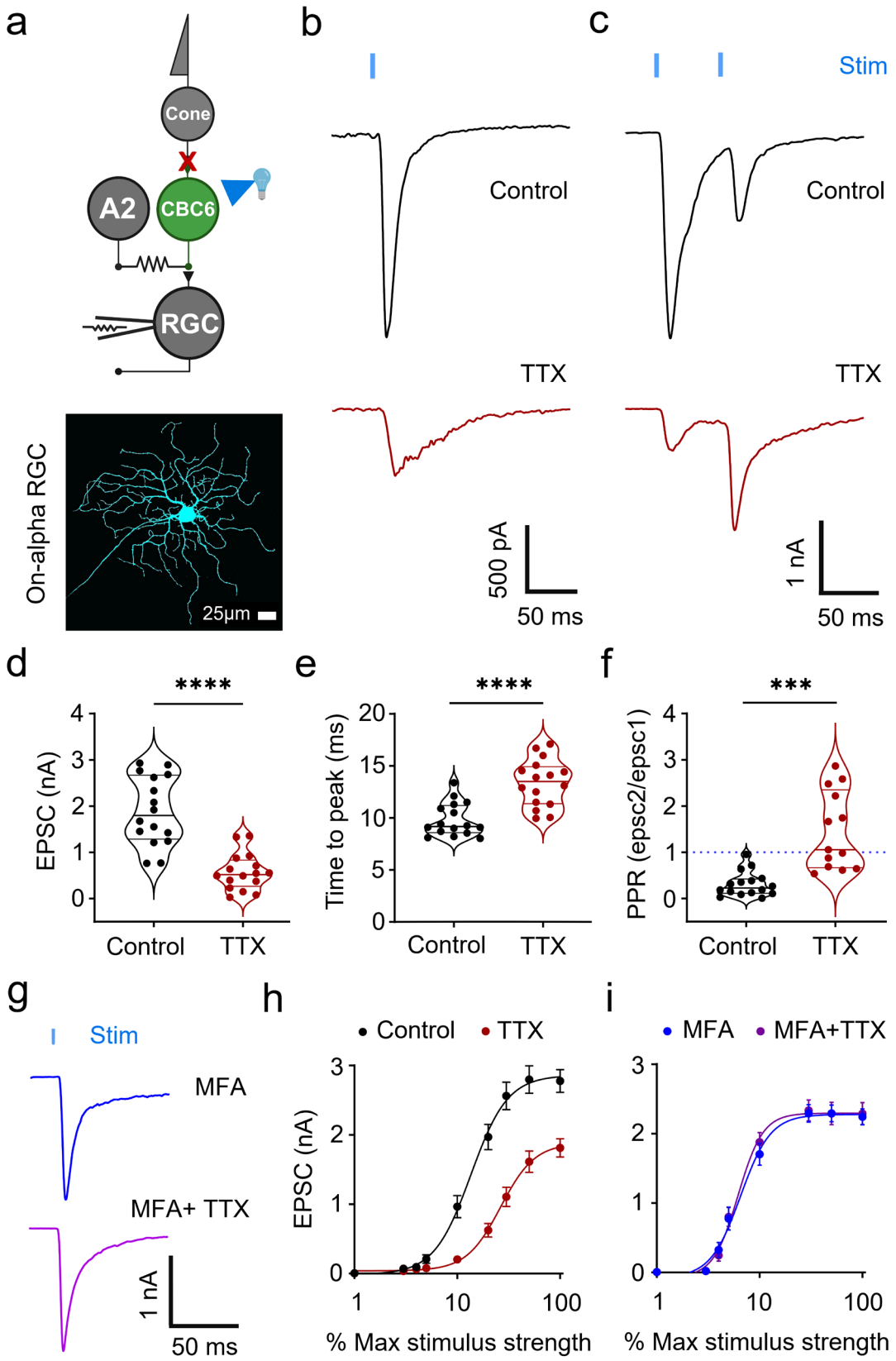

Figure 2. NaV channel-mediated excitability, spreading through gap junctions, amplifies synaptic output of CBC6 cells. a) Retinal circuit diagram showing the experimental arrangement. Full-field light flashes were used to optogenetically stimulate CBC6 cells and whole-cell patch clamp recordings were obtained from On-

212 alpha RGCs to measure evoked EPSCs. **b)** EPSCs elicited by a single flash (2 ms)
213 were reduced in amplitude and slowed by adding TTX. **c)** EPSCs elicited by a pair of
214 flashes (inter-stimulus interval=50ms) decremented without TTX but grew in amplitude
215 with TTX. **d-e)** Violin plots showing group data for **d)** amplitude and **e)** time-to-peak of
216 EPSCs elicited by a single stimulus without or with TTX. Note that TTX reduced the
217 EPSC amplitude by almost 70% (control=1894 ± 185 pA; TTX=574 ± 99 pA; n=16
218 each; p<0.0001); unpaired t-test), and slowed the peak by almost 50% (control=9.8 ±
219 0.4 ms; TTX=13.4 ± 0.6 ms; n=16 each; p<0.0001; unpaired t-test). (**f)** Group data for
220 paired-pulse ratio (PPR) of EPSCs elicited by pairs of stimuli without or with TTX. Note
221 that TTX changed PPR from depressing to facilitating (PPR: control=0.31 ± 0.07, n=16;
222 TTX=1.46 ± 0.23, n=13; p=0.0003; unpaired t-test). **g)** Pre-treatment with MFA to
223 uncouple gap junctions eliminated the effect of TTX on EPSCs, consistent with removal
224 of the A2 amplifier. **h)** The stimulus-response relationship of the CBC6 to RGC
225 synapse, obtained by varying optogenetic stimulus strength and measuring evoked
226 EPSCs. In TTX, stronger stimuli were required to evoke equivalent responses and
227 saturating EPSC amplitude was decreased (two-way ANOVA; treatment × stimulus
228 strength: F(2,69)=19.31; p<0.0001; control, n=16; TTX, n=18). **i)** Pre-treatment with
229 MFA eliminated the effect of TTX on CBC6 synaptic output (two-way ANOVA;
230 treatment × stimulus strength: F(2,41)=0.2795; p=0.7866; No TTX, n=11; TTX, n=12).
231 Violin plots depict median, 25th and 75th quartiles. Data in h, i are mean ± sem.

232 This raises the possibility that the effects of TTX on CBC6 synaptic output might involve
233 NaV channels in one or more wf-ACs, rather than, or in addition to, A2 cells. To test
234 this possibility, we blocked chemical synaptic inhibition with antagonists of glycine,
235 $GABA_A$ and $GABA_C$ receptors. We found that neither the peak optogenetic EPSC nor
236 its rise time were altered under these conditions (Extended Data Fig. 3b, c). Blocking
237 inhibition did slow the decay of the EPSC (Extended Data Fig. 3b, d), consistent with
238 the polysynaptic wf-AC pathway exerting feedback inhibition onto bipolar cell terminals
239 with a delay[36]. TTX reduced the peak amplitude of the EPSC to the same extent
240 whether or not chemical inhibition was blocked (Extended Data Fig. 4). These results
241 suggest that amplification of rapid synaptic transmission from CBC6 cells to On-alpha
242 RGCs involves A2 amacrine cells rather than wf-ACs.

243 To further verify the role of NaV channels in A2 cells as amplifiers of CBC6 synaptic
244 output we used QX-314, an open-channel blocker of the pore of voltage-gated ion
245 channels, including NaVs. As before, we optogenetically stimulated CBC6 cells and
246 recorded EPSCs in an On-alpha RGC, but we conducted this experiment in retinal
247 slices (200 µm), to reduce the number of CBC6 cells and A2 cells involved in
248 generating the RGC response.

249 First, we obtained a baseline EPSC (Fig. 3a, left). Then we impaled an A2 cell with a
250 sharp pipette containing QX-314 (1 mM) together with the fluorescent dye Alexa 594.

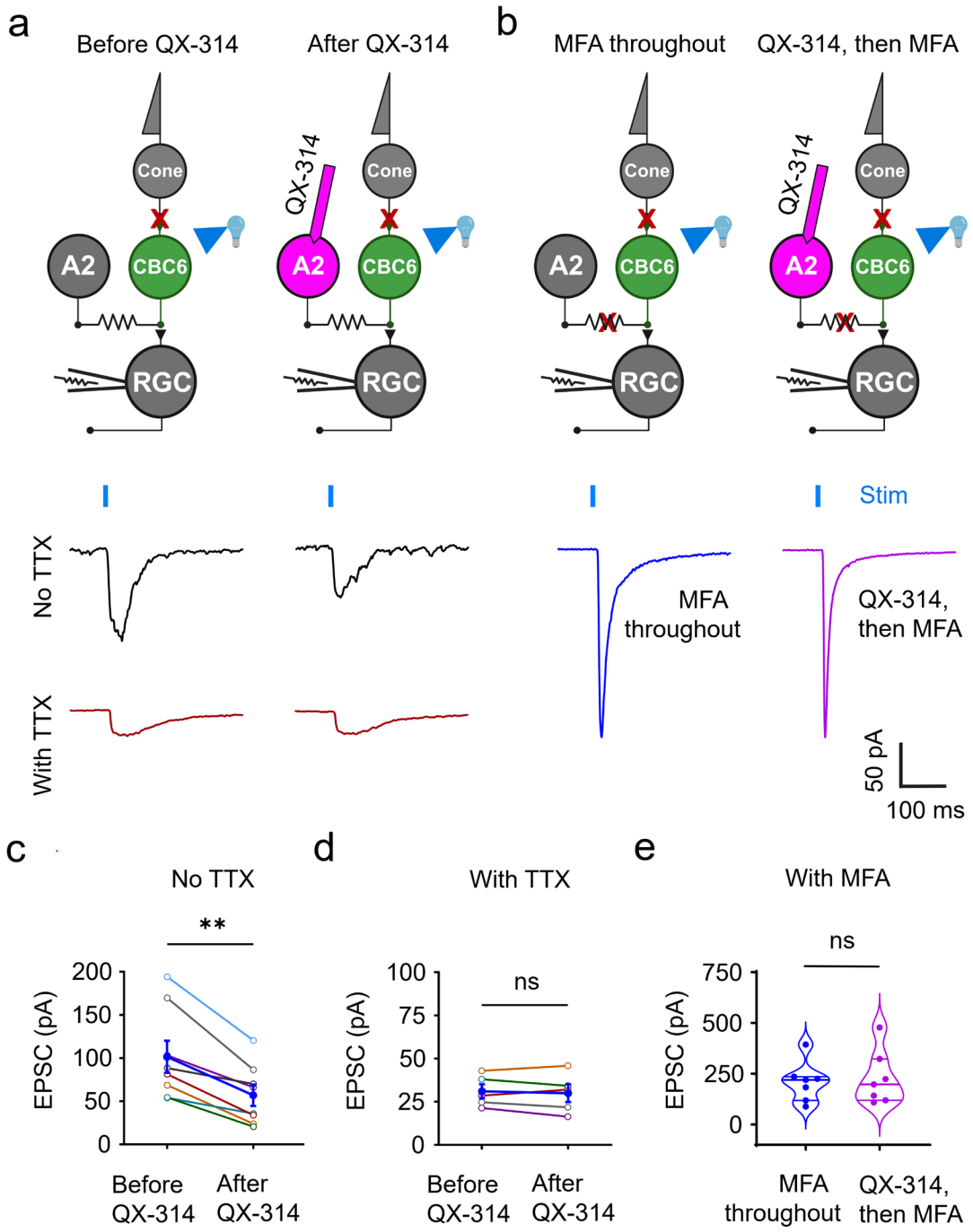

251 **Figure 3. Contribution of a single A2 cell to amplifying CBC6 synaptic output. a)**
252 Top: Retinal circuit diagram showing experimental arrangement. CBC6 cells were
253 optogenetically stimulated in a retinal slice, eliciting EPSCs in RGCs, before and after
254 injecting QX-314 into a single A2 amacrine cell with a sharp electrode. Bottom: Without
255 TTX in the bathing solution, EPSCs in the RGC were reduced following QX-314
256 injection. However, with TTX in the bathing solution, QX-314 injection had no effect.
257 **b)** Top: Retinal circuit diagram, showing experimental arrangement. To control for
258 possible diffusion of QX-314 from the A2 cell into the CBC6 cell, at 10 min after QX-
259 314 injection, MFA was applied to uncouple gap junctions connecting the A2 cell to
260 CBC6 cells. Bottom: EPSCs elicited after QX-314 injection followed by MFA treatment
261 did not differ from EPSCs elicited in MFA-treated slices without QX-314 injection,
262 suggesting no significant effect of QX-314 that might have entered CBC6 cells. **c)**
263 Without TTX, QX-314 injection reduced EPSC amplitude (before QX-314 = 102 ± 19
264 pA; after QX-314=57 ± 12 pA; n=8 each, p=0.0011; paired t-test). **d)** With TTX, QX-
265 314 injection had no effect (before QX-314=31 ± 4 pA; after QX-314=30 ± 5 pA; n=5
266 each, p=0.5723, paired t-test). Each thin line represents the same RGC recording,
267 before and after QX-314, The thick black line represents mean responses across all
268 RGCs. **e)** Group data indicate that QX-314 injection into A2 cells is inconsequential
269 when gap junctions are uncoupled (before QX-314=227 ± 50 pA; after QX-314=207 ±
270 37 pA, n=7 each, p=0.7527, unpaired t-test).

271 In every case, the amplitude of the EPSC was decreased significantly after introducing
272 QX-314 as compared to before (Fig. 3c). QX-314 injection had no effect on the EPSC
273 in control experiments in which TTX was present throughout the experiment (Fig. 3a,
274 d). We were concerned that some of the QX-314 injected into the A2 cell had diffused
275 through the gap junctions into the CBC6 terminal, where it might advertently block their
276 voltage-gated channels, including Ca^{2+} channels, thereby reducing evoked
277 neurotransmitter release apart from affecting NaV channels.

278 To exclude this possibility, we measured optogenetic EPSCs before and after QX-314
279 injection, and then again, after treating with MFA to uncouple the gap junctions (Fig.
280 3b). If QX-314 had crossed from the A2 cell into the CBC6 terminal, the evoked EPSC
281 would have been smaller than if QX-314 had not been injected into the A2 cell in the
282 first place. However, we observed no difference in EPSC amplitude elicited by

283 activating uncoupled CBC6 cells, whether an A2 had received QX-314 or not (Fig. 3e),
284 inconsistent with local channel blockade within a CBC6 cell. Taken together, these
285 experiments definitely identify the A2 cell as the source of NaV-mediated excitability
286 that amplifies CBC6 synaptic transmission to RGCs.

287 By removing NaV-mediated amplification, one might expect that uncoupling CBC6 cells
288 from A2 cells would reduce the amplitude of EPSCs recorded in the RGCs. However,
289 we found that EPSC amplitude either increased or remained unaltered after treatment
290 with MFA (Fig. 2, 3). Consistent with a previous study[37], our experiments revealed that
291 gap junctions set the resting membrane resistance of On-CBCs including CBC6 cells,
292 and that depolarization, whether elicited by physiological or optogenetic stimuli, is
293 reduced by this gap junctional shunt (Supplementary information). Activation of NaV
294 channels in the A2 cell helps offset this signal reduction, ensuring that depolarization
295 of CBC6 terminals can effectively activate voltage-gated Ca^{2+} channels and trigger
296 neurotransmitter release.

297 **Consequences of the A2 amplifier for spatial processing.**

298 The mouse retina exhibits a high degree of convergence, with ~6.7 million rods and
299 cones generating signals carried to the brain by ~50,000 RGCs[38]. Within the cone
300 CBC6 subcircuit, 2-3 cones converge onto each CBC6 cell dendritic tree[39], ~10 CBC6
301 cells normally converge onto each A2 amacrine cell[21,40], 5-10 A2s likely converge onto
302 a CBC6 cell, and 200-400 CBC6 cells converge on each On-alpha RGC[22]. We
303 evaluated how this circuit arrangement, combined with NaV-mediated A2 cell
304 excitability, influences spatial encoding by the circuit.

305 We started by optogenetically activating an array of CBC6 bipolar cells with a bar of
306 light while measuring the resulting compound EPSPs in an A2 amacrine cell (Fig. 4a).
307 The A2 cell was identified with the help of mCherry expression and visualized by dye-
308 filling with Alexa 594, which also enabled accurate positioning of the stimulus. We used
309 the same mixture of neurotransmitter receptor inhibitors described above to prevent
310 natural light responses of rods and cones from influencing the downstream circuity.

311 A narrow bar of light (18 μm) positioned either over the axodendritic tree of the A2 cell
312 or 90μm away from the A2 somata generated small EPSPs, which were unaffected by
313 adding TTX (control=5.55 ± 0.80 mV, n=14; TTX=6.07 ± 1.25 mV, n=13; p=0.9076).
314 TTX did not alter the response of A2 cells, irrespective of the location of the bar of light
315 (Fig. 4b-d). Stimulation with two bars of light positioned far apart (90 μm) generated an

316 EPSP that was roughly twice as large as a single bar and again, the response was
317 unaffected by TTX (control=13.02 ± 1.77 mV; TTX=8.84 ± 1.47 mV; n=6 each;
318 p=0.2629) (Fig. 4e, f). However, positioning the two bars immediately adjacent to one
319 another resulted in an EPSP that was 4-5-fold larger than from a single bar and almost
320 2-3-fold larger than predicted from linearly summing the responses (predicted=9.91 ±
321 1.00 mV; observed=24.33 ± 2.17 mV; n=8 each; p=0.0004).

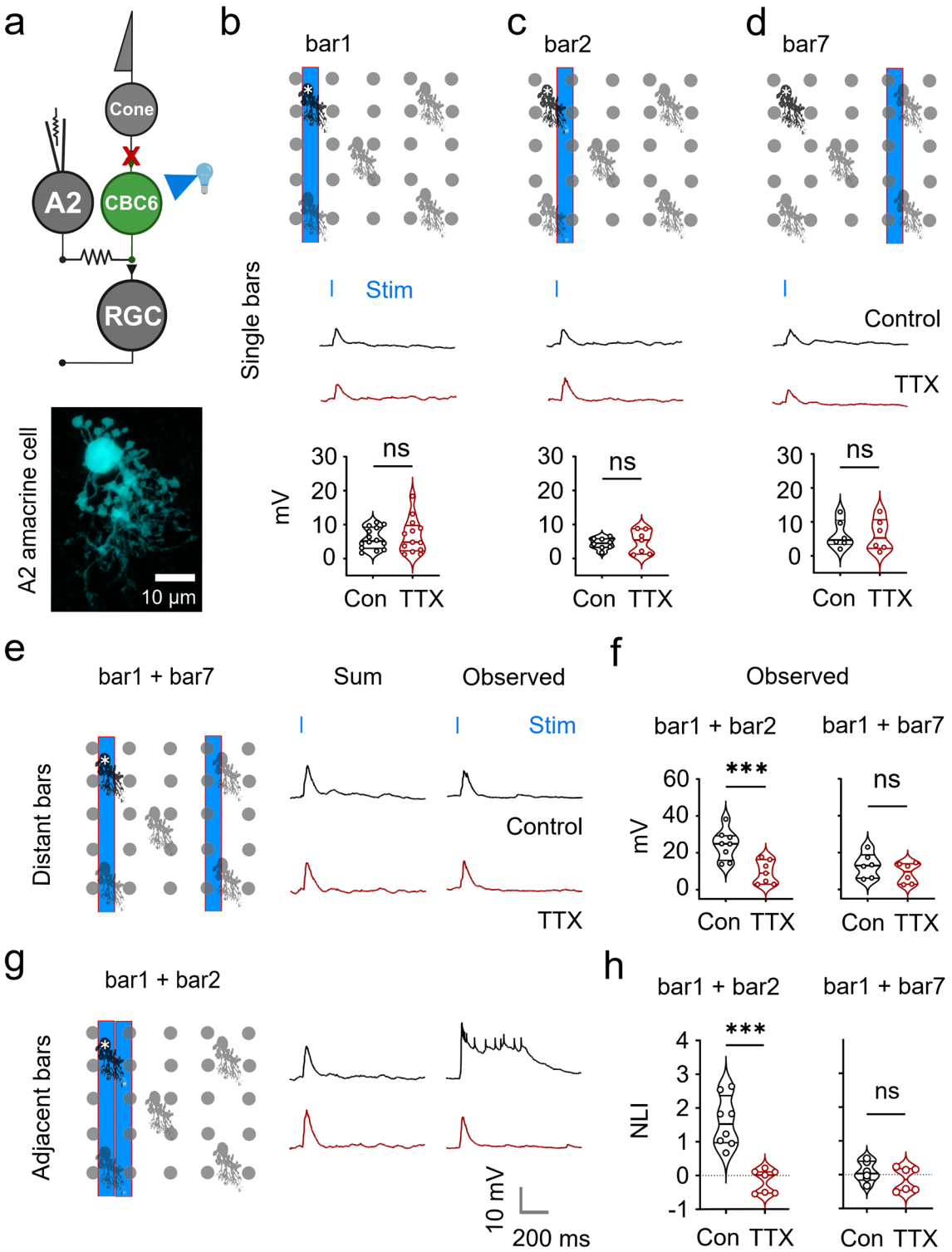

322 **Figure 4. NaV-mediated excitability in A2 cells results in supra-linear summation**
323 **of voltage responses driven by spatially adjacent CBC6 cells. a)** Retinal circuit
324 diagram, showing experimental arrangement. **b-d)** A narrow bar of light (18 µm wide,
325 360 µm long) was projected onto the retina to optogenetically stimulate rows of CBC6
326 cells at three different positions relative to the patch-clamped A2 cell; **b)** bar 1:
327 immediately over the A2 cell (asterisk), **c)** bar 2: 18 µm off-center from the A2 cell, or
328 **d)** bar 7: 90 µm off-center from the A2 cell. Membrane potential of the A2 cell was
329 allowed to "float" (i.e., not voltage-clamped) to enable recording of EPSPs and
330 associated regenerative depolarizations. Bottom panel shows group data and
331 variability of EPSP amplitudes evoked by each bar. Note that the amplitudes were
332 nearly the same at all three positions, and that TTX had no significant effect (bar1:
333 control=5.89 ± 0.83 mV, n=14; TTX=6.66 ± 1.37 mV, n=13; p=0.6441; bar2:
334 control=4.42 ± 0.42 mV, n=8; TTX=4.86 ± 0.90 mV, n=7; p=0.7597; bar7: control=6.29
335 ± 1.11 mV, n=6; TTX=6.17 ± 1.26 mV, n=6; p=0.9653; unpaired t-test in each case). **e,**
336 **g).** Results elicited by projecting pairs of bars on the flat-mount retinas. Two bars of
337 light, each 18 µm wide as in **b-d**, were separated either by 90 µm (distant) or 0 µm
338 (adjacent). The observed EPSPs for each is shown in comparison to the predicted
339 EPSP, calculated assuming linear summation of two of the single bar EPSP responses
340 shown in panels b-d. For distant bars, the observed peak response was similar to the
341 summed response and neither were affected by TTX. However, for adjacent bars, the
342 observed peak response was larger than the predicted summed response and it was
343 followed by a prolonged plateau potential with small spikes. **f)** Group data for each A2
344 cell recording, as depicted by the representative responses in e and g. Distant bars
345 (bar1 + bar7) produced EPSPs almost twice as a single bar, which were unaffected by
346 TTX (control=13.02 ± 1.77 mV, TTX=8.84 ± 1.47 mV, n=6 each; p=0.2629; unpaired t-
347 test). Adjacent bars (bar1 + bar2) produced 2-3-fold larger EPSPs than predicted
348 (observed=24.33 ± 2.17 mV, predicted=9.91 ± 1.00 mV, n=8 each; p=0.0004; paired t-
349 test), which was reduced substantially in the presence of TTX (observed: control=
350 24.33 ± 2.17 mV, n=8; TTX=9.45 ± 1.68 mV, n=7; p=0.0016; unpaired t-test). **h)** Group
351 data of the non-linearity index (NLI) of A2 cell responses in response to simultaneous
352 presentation of distant or adjacent bars. Distant bars produced either linear or sublinear
353 responses irrespective of TTX application (control=0.08 ± 0.08, TTX= -0.14 ± 0.09; p=
354 0.3939; Mann-Whitney test). Adjacent bars produced supralinear responses, which
355 were abolished by TTX (control=1.59 ± 0.20, TTX= -0.16 ± 0.09; p=0.0003; Mann-

356 Whitney test). Non linearity index was calculated as follows: EPSP (Observed –
357 Predicted)/Predicted. Values above and below 0 indicate supralinear and sublinear
358 responses, respectively.

359 Moreover, the EPSP was much longer-lasting (>than 500 msec), and it was followed
360 by a plateau potential with a train of small spikelets on top (Fig. 4g, h). Addition of TTX
361 eliminated the spikelets and the plateau potential, and brought the EPSP amplitude in
362 agreement with that predicted from linear summation (predicted=11.39 ± 1.49 mV;
363 observed=9.45 ± 1.68 mV; n=7 each; p=0.2497). Taken together, these results suggest
364 that NaV-mediated excitability of A2 cells leads to non-linear summation of synaptic
365 inputs from multiple CBC6 cells, if those CBC6 cells are close enough to converge onto
366 the same A2 cell.

367 Next, we asked whether the preference for spatially adjacent stimuli, activating
368 neighboring CBC6 cells, also applies to RGCs. We used the same bars of light to
369 stimulate CBC6 cells, but recorded EPSCs in On-alpha RGCs under voltage-clamp
370 (Fig. 5a). Individual bars of light positioned at various locations with respect to the
371 dendritic tree of an RGC generated similar EPSCs and TTX had no significant effect
372 (control=151 ± 10 pA, n=7; TTX=171 ± 9.7 pA, n=8; p=0.0891). TTX did not alter the
373 response of On-alpha RGCs irrespective of the location of single bars (Fig. 5b-d). Two
374 bars, positioned far apart (90μm) resulted in EPSCs that were roughly twice as large,
375 which were unaffected by adding TTX (control=239 ± 27 pA, n=7; TTX=286 ± 32 pA,
376 n=8; p=0.2789) (Fig. 5e). However, two adjacent bars of light resulted in EPSCs that
377 were nearly 2-fold larger than predicted (predicted=322 ± 22 pA; observed=614 ± 48
378 pA; n=7 each; p=0.0156). Once again, the non-linear summation of the response was
379 eliminated by adding TTX (predicted=351 ± 26 pA; observed=333 ± 29 pA; n=8 each;
380 p=0.4916) (Fig. 5f-g), implicating NaV channels in A2 amacrine cell as the critical
381 source.

382 A2 amacrine cells have a dendritic tree that is roughly 36 μm in diameter. However,
383 A2 cells not only couple to CBC6 cells through gap junctions, they are also coupled by
384 gap junctions to one another. To determine the minimum bar spacing necessary to
385 generate supra-linear summation measured in RGCs, the distance between the bars
386 was narrowed progressively until they were adjacent. We found that the response to
387 bars of light increased supra-linearly at inter-bar distances <72 μm, with a half-maximal
388 effect at about 36 μm (Fig. 5h). This suggest that simultaneously activated CBC6 inputs

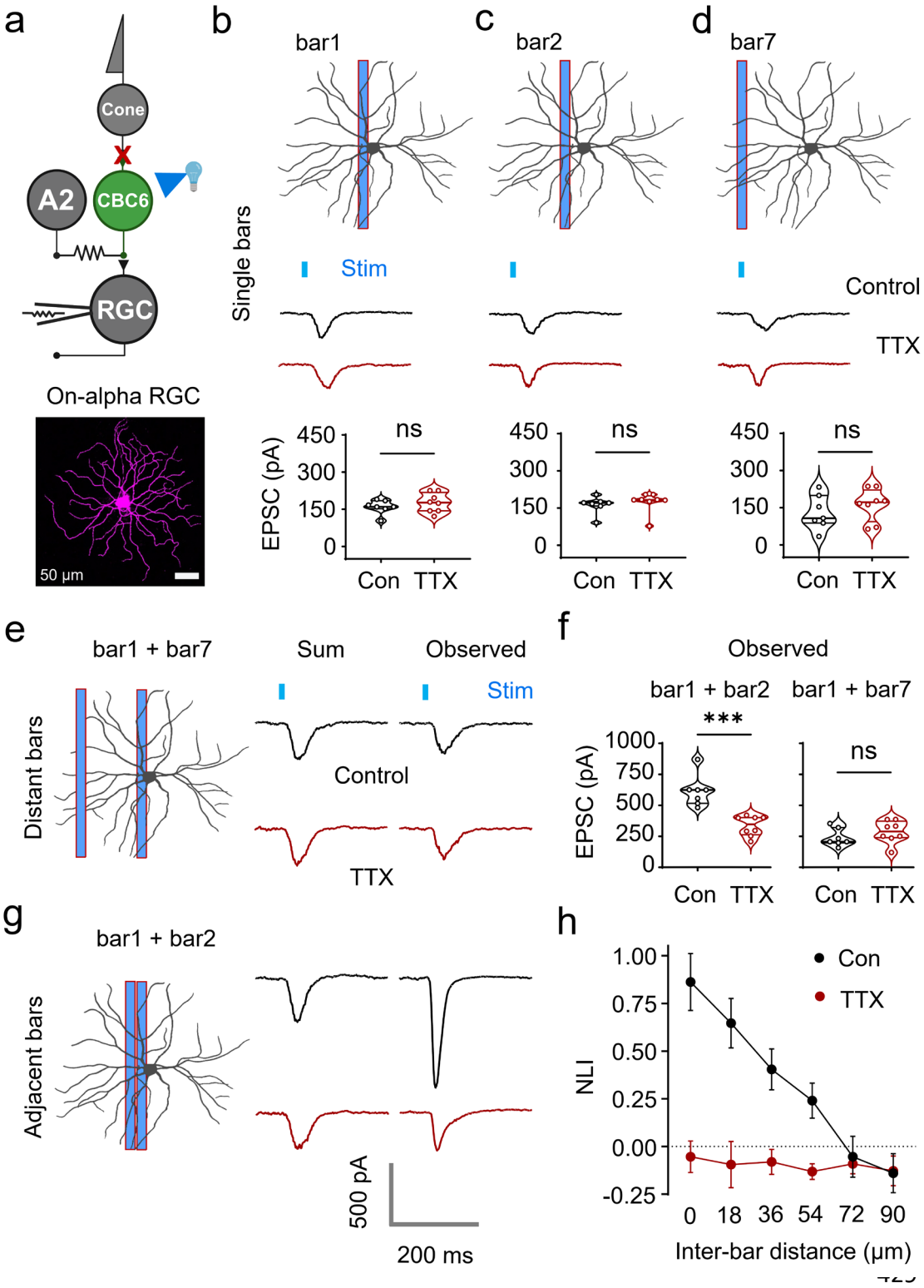

Figure 5. NaV-mediated excitability amplifies optogenetically-elicited synaptic output from spatially adjacent CBC6 cells to an individual RGC. a) Retinal circuit diagram, showing experimental arrangement. b-d) A narrow bar of light (18 µm wide, 360 µm long) was projected onto the retina to optogenetically stimulate rows of CBC6 cells at three different positions relative to the patch-clamped On-alpha RGC; b) bar 1: immediately adjacent to the RGC soma, c) bar 2 : 18 µm off-center from the RGC soma

436 , or d) bar 7: 90 μm off-center from the RGC soma. Bottom panel shows group data
437 and variability of EPSC amplitudes evoked by each bar. Note that the amplitude was
438 nearly the same at all three positions, and that TTX had no significant effect (bar1:
439 control=160 ± 10 pA, n=7; TTX=176 ± 14 pA, n=8; p=0.3562; unpaired t-test; bar2:
440 control=163 ± 12 pA, n=7; TTX=174 ± 14 pA, n=8; p=0.0693; Mann-Whitney test; bar7:
441 control=131 ± 24 pA, n=7; TTX=162 ± 23 pA, n=8; p=0.3932; unpaired t-test) **e, g).**
442 Results elicited by projecting pairs of bars onto the retina. Two bars of light, each 18
443 μm wide as in **b-d**, were separated either by 90 μm (distant) or 0 μm (adjacent). The
444 observed EPSCs for each is shown in comparison to the predicted EPSC, calculated
445 assuming linear summation of two of the single bar EPSC responses shown in panels
446 b-d. **f)** Group data for each On-alpha RGC recording, as depicted by the representative
447 responses in e and g. Distant bars (bar1 + bar7) produced EPSCs almost twice as a
448 single bar, which were unaffected by TTX (control=239 ± 27 pA, n =7; TTX=286 ± 32
449 pA, n=8; p=0.2789; unpaired t-test). Adjacent bars (bar1 + bar2) produced almost 2-
450 fold larger EPSCs than predicted (observed=614 ± 48 pA, predicted=322 ± 22 pA, n=7
451 each; p=0.0156; Wilcoxon signed rank test), which was reduced substantially in the
452 presence of TTX (observed: control=614 ± 48 pA, n=7; TTX=333 ± 29 pA, n=8;
453 p=0.0005; unpaired t-test). **h)** Group data showing the non-linearity index (NLI) of On-
454 alpha RGC responses elicited by bars separated by different distances. Note that the
455 NLI was minimal at separations ≥ 72 μm, maximal for adjacent bars and half-maximal
456 at ~36 μm. The observed supralinear responses were abolished in the presence of
457 TTX (two-way ANOVA; treatment × bar separation: F(2, 25)=11.51; p=0.0002; control,
458 n=6; TTX, n=7). Data in h are mean ± sem.

459 are most likely to be amplified if the inputs converge on a single A2 cell of 36 μm
460 diameter, although inputs onto a neighboring A2 cell also contribute to the
461 amplification, but to a lesser extent. Taken together, these findings suggest that spatial
462 summation of excitatory inputs from CBC6 cells onto a single A2 cell is necessary to
463 bring the cell above action potential threshold, thereby triggering amplification of
464 synaptic transmission from CBC6 cells to RGCs.

465 **A2 amacrine-cell mediated amplification applies to natural light responses**
466 **triggered by cone photoreceptors**.

467 Up until this point, we have relied exclusively on optogenetic stimulation of CBC6 cells
468 to elicit light responses in A2 amacrine cells and On-alpha RGCs. We wondered
469 whether A2 cell amplification also applies to light responses triggered naturally by cone
470 photoreceptors (Fig. 6a). To address this question, we omitted all of the
471 pharmacological blockers used in our other experiments, and bathed the retina in
472 normal physiological saline. Dissection of the retinas was performed under photopic
473 light conditions that presumably photobleached or saturated rods, eliminating their light
474 responses[41,42]. Thereafter, these experiments were carried out in mesopic background
475 light following the recovery of cone photoreceptors (see Methods).

476 We stimulated cones with an array of 9 spots of light, each ~36 μM in diameter. The 9
477 spots were either widely dispersed, with each spot 72 μm from its nearest neighbor
478 (left, Fig. 6b), or tightly clustered, with the 9 spots immediately adjacent to one another
479 (left, Fig. 6c). In both cases, the array of spots was positioned to fall within an area
480 delineated by the dendritic tree of the On-alpha RGCs. In principle, both dispersed and
481 clustered stimulus arrays should activate the same number of pre-synaptic BCs, and
482 with no extra amplification, should generate the same summated EPSC.

483 Not surprisingly, the dispersed array of spots generated a moderate-sized summated
484 EPSC that was unaffected by adding TTX (Fig. 6b, f). However, we found that the
485 clustered array generated a summated EPSC that was almost twice as large as
486 predicted (dispersed=266 ± 31 pA; clustered=573 ± 51 pA; n=8 each; p=0.0002) and
487 had a faster rise time (dispersed=108.2 ± 6.1 ms; clustered=87.4 ± 5.7 ms; n=8 each;
488 p=0.0056) (Fig. 6c, e). TTX had a dramatic effect on the response to the clustered
489 array, slowing its rise time and reducing its peak amplitude to match that elicited by the
490 dispersed array (Fig. 6h, i).

491 Shifting the dispersed and clustered arrays to different positions within the dendritic
492 tree collecting area of the RGC made little difference to the relative amplitudes of
493 summated EPSCs that were elicited. The response to the clustered array was always
494 about twice as large as the dispersed array, whether the cluster fell on BCs cells near
495 the center or the periphery of the RGC's dendritic tree (Fig. 6d, g). The simplest
496 interpretation of these results is that activation of neighboring cones results in
497 activation of spatially clustered BCs, which converge onto common A2 cells, resulting

498 in NaV-mediated synaptic amplification of CBC6 and potentially other On-CBCs output,
499 whereas activation of dispersed cones does not lead to amplification.

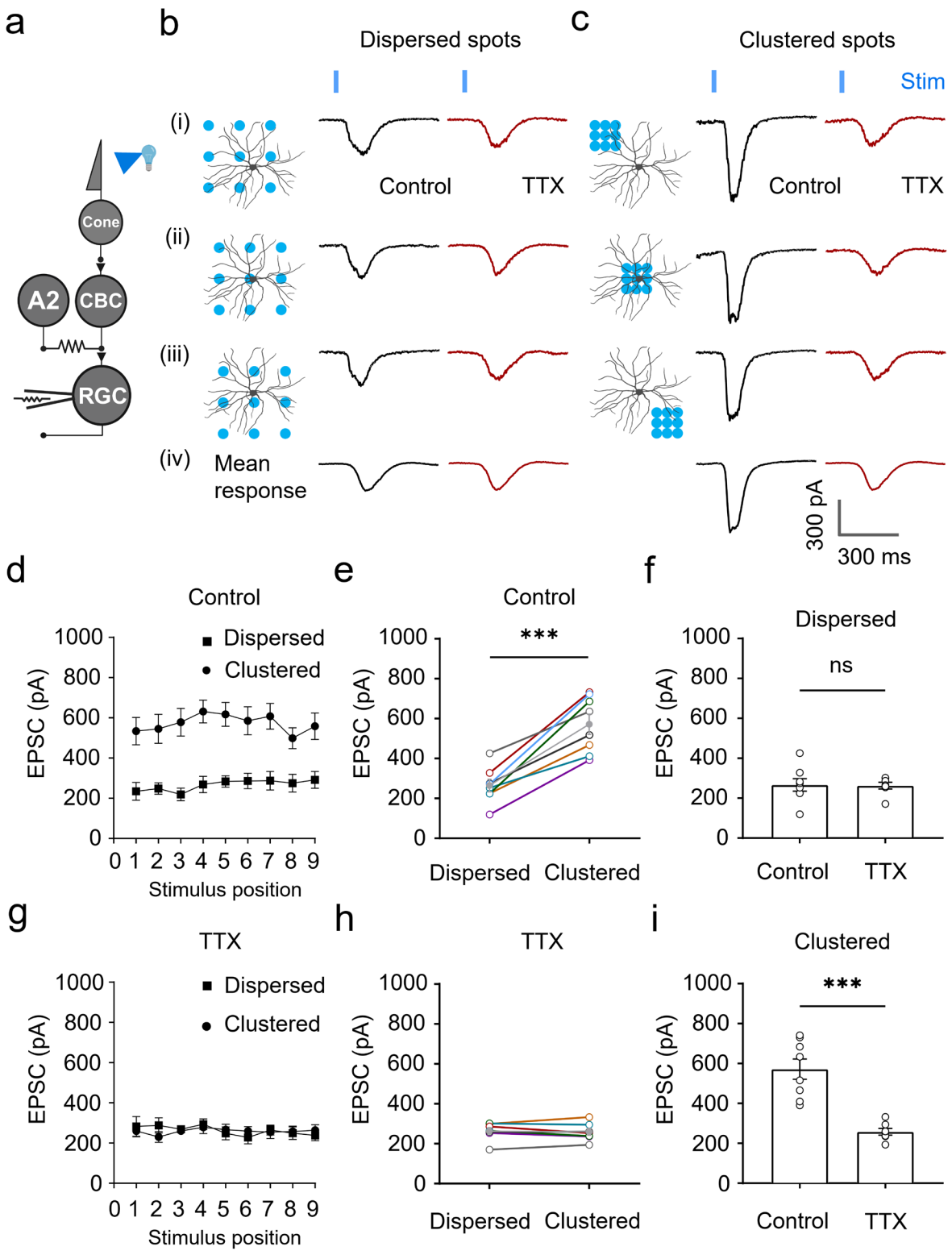

500 **Figure 6. NaV-mediated excitability amplifies natural RGC light responses driven**
501 **by spatially adjacent cones. a)** Retinal circuit diagram, showing experimental
502 arrangement. The light-adapted retina was exposed to spots of light to activate cones
503 while EPSC responses from an RGC were recorded under voltage clamp. **b)** A set of
504 9 dispersed spots, each 36 µm in diameter and separated by 72 µm was presented to
505 the retina, all confined within the dendritic tree territory of a patch-clamped RGC that
506 had been filled with fluorescent dye. The set of dispersed spots were presented in nine
507 different positions relative to the RGC dendritic tree and the responses to three of which
508 (i-iii) are shown. Note that all 3 positions elicited similar EPSCs, as did the mean
509 response from all positions (iv). All of the responses were unaffected by TTX. **c)**
510 Responses to the same 9 spots of light, but clustered to be immediately adjacent to
511 one another. The clustered spots were presented in nine different positions and the
512 responses to three (i-iii) are shown. Note that all 3 positions elicited larger EPSCs
513 which were all reduced by TTX. **d, g)** Responses to dispersed and clustered spots
514 without and with TTX at each position (two-way ANOVA; stimulus type × stimulus
515 location: control, $F(4,56)=0.8276$, $n=8$, $p=0.5124$; TTX, $F(2,23)=0.5830$, $n=7$,
516 $p=0.5568$; stimulus type: control, $F(1,14)=26.50$, $n=8$, $p=0.0001$; TTX, $F(1,12)=0.0194$,
517 $n=7$, $p=0.8916$). **e, h)** Average response at all 9 positions. Note that the clustered spots
518 produced almost 2-fold larger EPSCs compared to the dispersed spots (clustered=573
519 ± 51 pA, dispersed=266 ± 31 pA, n=8 each; p=0.0002; paired t-test). In the presence
520 of TTX, however, clustered spots elicited smaller EPSCs which were roughly the same
521 size as produced by the dispersed spots (clustered=259 ± 16 pA, dispersed=262 ± 16
522 pA, n=7 each; p=0.7350; paired t-test). (**f, i)** Comparison of all responses to dispersed
523 and clustered spots, without and with TTX (dispersed: control=266 ± 31 pA, n=8,
524 TTX=262 ± 16 pA, n=7; p=0.9215; unpaired t-test; clustered: control=573 ± 51 pA, n=8,
525 TTX=259 ± 16 pA, n=7; p=0.0003; unpaired t-test). Data in f, i are mean ± sem. These
526 experiments were carried out in mesopic background (758 R*/rods/s) at 100 %
527 contrast. The duration of stimulus was 10 ms.

528 All of the above experiments were carried out in mesopic lighting conditions, near cone
529 threshold[43] (758 R*/rods/s). If A2-mediated amplification is an important mechanism
530 for object detection, one might expect weaker amplification in brighter light. To evaluate
531 the effect of lighting, we repeated the dispersed vs. clustered spot experiment while
532 varying the intensity of both the background (I_B) and the spot (I_S) to maintain a constant

533 contrast (I_s/I_B = 2.0) (Fig. 7a-e). In mesopic lighting (background= 758 R*/rods/s),
534 dispersed spots generated a small EPSC (Fig. 7c, d), but clustered spots generated a
535 much larger EPSC (peak amplitude 2.2-fold larger). In low photopic light (background=
536 3,790 R*/rods/s, clustered spots elicited EPSC that were only modestly larger than with
537 dispersed light (1.2-fold larger).

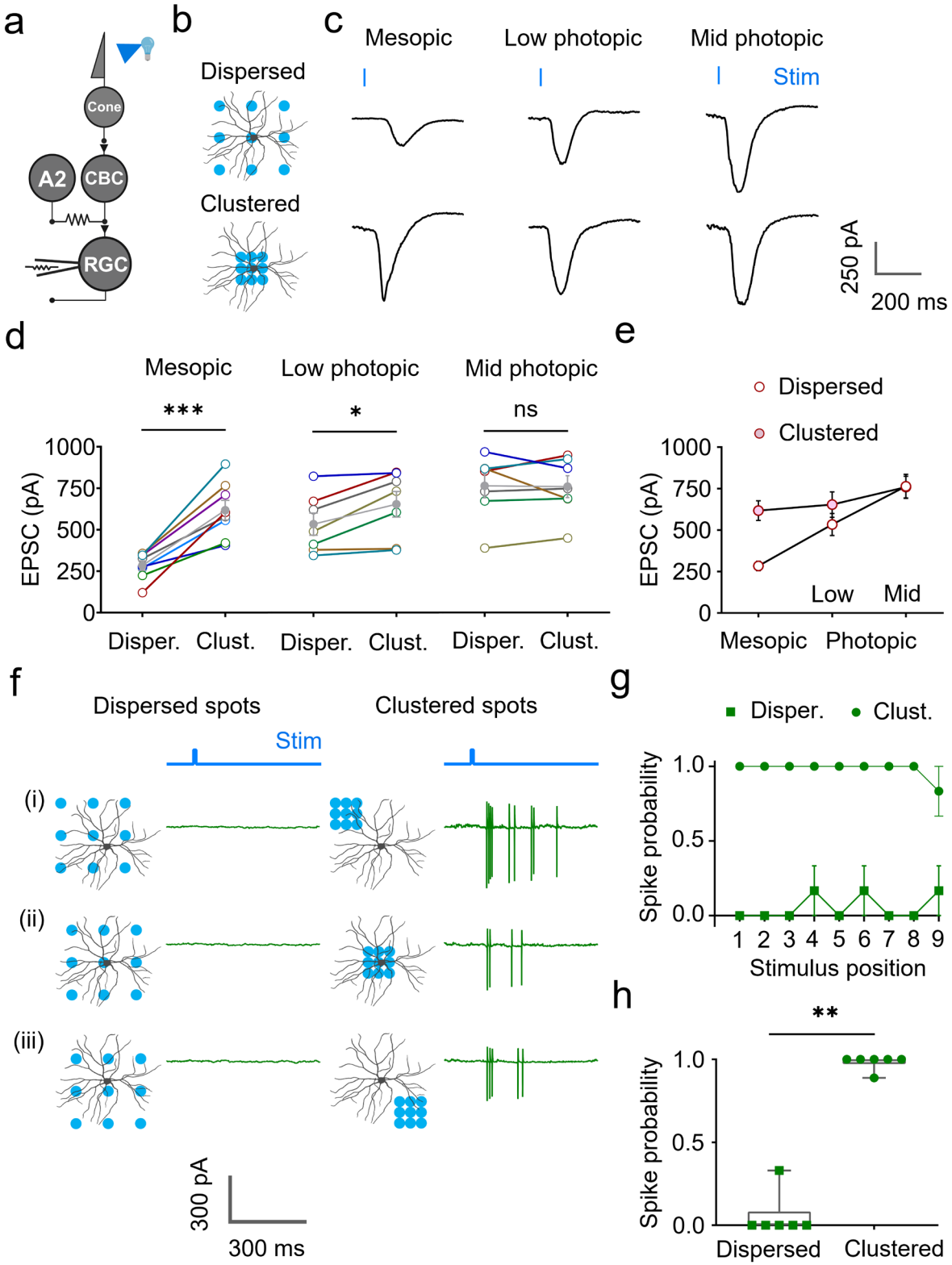

538 **Figure 7. Amplification is largely restricted to mesopic conditions. a)** Retinal
539 circuit diagram, showing experimental arrangement. The retina was exposed to spots
540 of light to activate cones while EPSC (c-e) or spike responses (f-h) from an On-alpha
541 RGC were recorded. **b)** Dispersed or clustered spots were presented to the retina in
542 one position **c)** EPSC recordings from an On-alpha RGC in response to the dispersed
543 spots (top) and the clustered spots (bottom) with increasing background light: mesopic
544 (758 R*/rods/s), low-photopic (3790 R*/rods/s) and mid-photopic conditions (18950
545 R*/rods/s). **d)** Clustering of spot stimuli strongly amplified responses in mesopic
546 background (dispersed=283 ± 29 pA, clustered=617 ± 59 pA, n=8 each, p=0.0003,
547 paired t-test), weakly in low-photopic background (dispersed=533 ± 67 pA,
548 clustered=653 ± 77 pA, n=7 each, p=0.0169, paired t-test) and not at all in mid-photopic
549 background (dispersed=763 ± 73 pA, clustered=759 ± 66 pA, n=7 each, p=0.9056,
550 paired t-test). Open circles represent individual RGC responses; filled grey circles
551 represent the mean response from all recorded RGCs. **e)** Background alters responses
552 to the dispersed spots but not the clustered spots. EPSC amplitude to the dispersed
553 spots increased from mesopic to low-photopic to mid-photopic background (One-way
554 ANOVA; background light: F(2,19)=18.12, p=<0.0001). In response to the clustered
555 spots, the size of EPSCs did not change across these backgrounds (One-way ANOVA;
556 background light: F(2,19)=1.198, p=0.3236). Note that unlike the response to the
557 dispersed spots, the response to the clustered spots was already nearly-maximal
558 EPSCs in the mesopic background. For these experiments, contrast was 100 % in all
559 three conditions and the duration of stimuli was 10 ms. **f)** Left: The dispersed spots
560 were presented in nine different positions and the responses to three (i-iii) are shown.
561 Note that none of the stimulus positions elicited spikes. Right: The clustered spots were
562 presented in nine different positions and the responses to three (i-iii) are shown. Note
563 that all 3 stimulus positions elicited spikes. **g)** Mean probability of spiking in response
564 to the dispersed and the clustered spots at all 9 positions (two-way ANOVA; stimulus
565 type × stimulus location: F(2,17)=0.8197, n=6 each, p=0.4384; stimulus type:
566 F(1,10)=243.2, n=6 each, p<0.0001). **h)** Cell-wise probability of spiking in responses
567 to the dispersed and the clustered spots (dispersed=0.06 ± 0.06, clustered=0.98 ±
568 0.02; n=6 each; p=0.0022, Mann-Whitney test). For panels g and h, error bars denote
569 ± sem. Note that these cell-attached spike recordings were performed in mesopic
570 background at 100% contrast. Spiking probability denotes the fraction of stimulus that
571 elicited spikes, which could vary between 0 to 1.

572 In brighter photopic light (background= 18,950 R*/rod/s), clustered spots generated
573 EPSC responses with the same peak amplitude as dispersed spots (Fig. 7c, d). In
574 general, RGC responses to dispersed spots gradually increased with increasing
575 intensity, while the response to clustered spots remained largely unchanged (Fig. 7e).
576 These results indicate that A2 cells strongly amplify responses in mesopic conditions,
577 mildly in low photopic conditions. and not at all in mid-photopic or brighter conditions.
578 The constancy of responses to clustered stimuli across several log units of light
579 intensity is consistent with A2 cell-mediated amplification playing an important role in
580 object recognition.

581 Finally, we asked whether the spatial clustering preference exhibited by A2 cells affects
582 the spike output of RGCs, the critical signals for sensory processing by the brain and
583 visual perception by the animal. We obtained "loose patch" extracellular recordings
584 from On-alpha RGCs, and quantified the probability of spikes occurring in response to
585 dispersed or clustered spots of light that activated cone photoreceptors. Once again,
586 we found a strong preference for clustered stimuli, independent of the specific location
587 within the center of the RGC's receptive field (Fig 7f-h). This finding is consistent with
588 the A2 amplifier playing an important role in tuning the response properties of On-alpha
589 RGCs to respond more strongly to spatially distinct objects rather than spatially
590 uncorrelated stimuli.

591 Up until now, our focus has been on the role of A2 amacrine cells in amplifying
592 excitatory synaptic transmission between CBC6 cells and On-alpha RGCs. However,
593 this is only one of many On-subcircuits in the inner retina. Several other types of On-
594 cone bipolar cells are also electrically coupled to A2 amacrine cells [21] and along with
595 CBC6 cells, provide inputs to most of the >20 On-RGCs in the mouse retina[20,44]. To
596 test whether NaV channel-mediated spatial thresholding from A2 cells applies to other
597 types of On-RGCs, we obtained patch clamp recordings from RGC somata that were
598 located very close to presumed On-alpha RGC somata (within <50 µm). This makes
599 these cells very unlikely to also be On-alpha RGCs, which are spaced at a regular inter-
600 somatic distance in the mouse retina[45]. Dye-filling confirmed that the soma size and
601 the dendritic tree pattern of these "non-alpha" On-RGCs were distinct from On-alpha
602 RGCs (Fig 8 a). As we used Kcng4-cre X Ai9 mice for recording natural light responses,
603 identification of alpha-RGCs, and therefore non-alpha RGCs, was more straightforward
604 in this case as tdTomato expression was confined to alpha-RGCs[46].

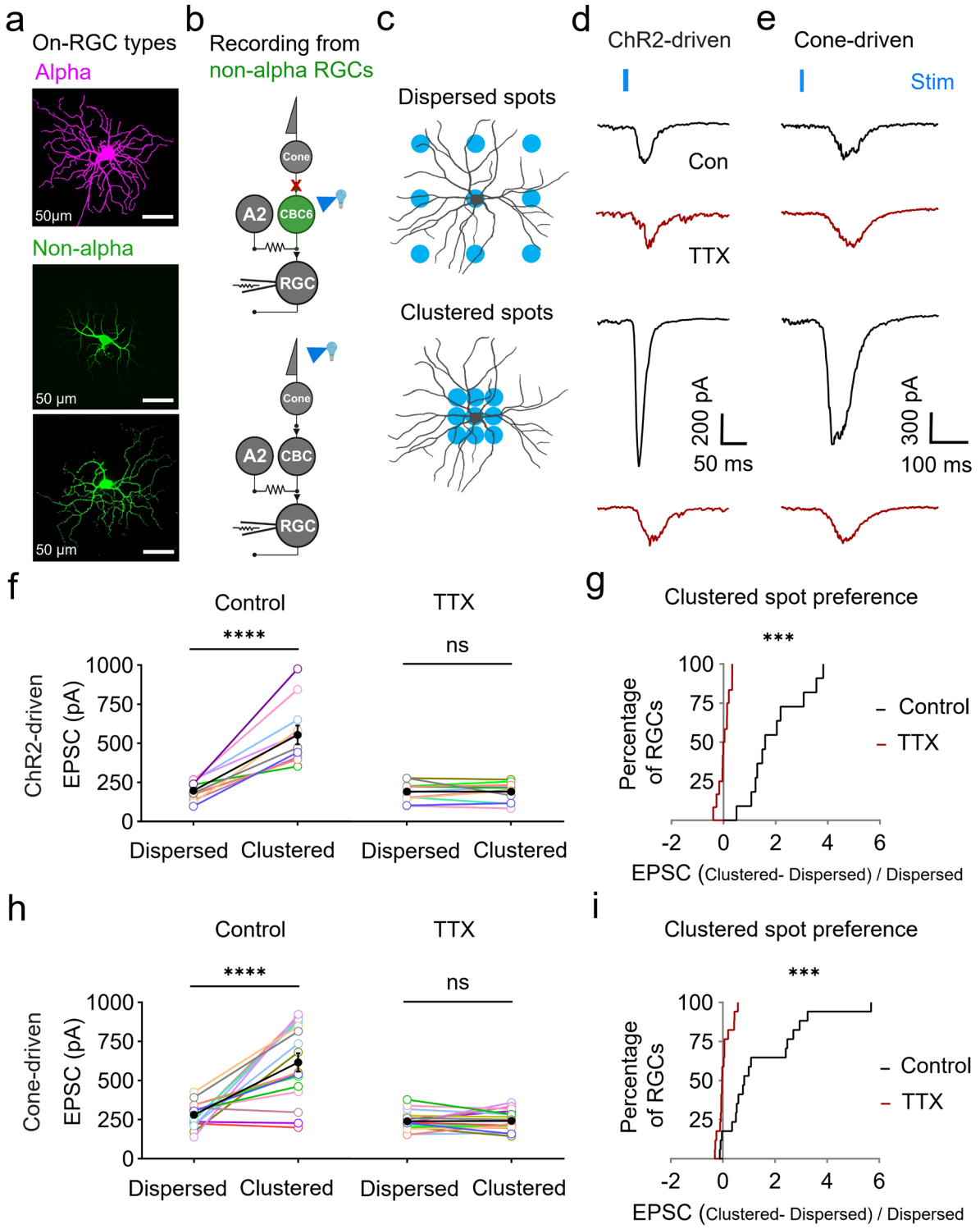

605 **Figure 8. Multiple types of On-RGCs prefer spatially clustered stimuli, mediated**
606 **by NaV-mediated excitability of A2 amacrine cells. a)** Examples of dye-filled alpha
607 and non-alpha On-RGCs. **b)** Retinal circuit diagram, showing experimental
608 arrangement. The retina was photostimulated optogenetically, with ChR2 expressed in
609 CBC6 cells and input from photoreceptors blocked (top), or naturally, by
610 photostimulating cones (bottom). EPSC responses were recorded in non-alpha On-

611 RGCs. **c)** Dispersed or clustered stimuli were presented as described in previous
612 figures. **d, e)** Responses in non-alpha On-RGCs to optogenetic photostimulation of
613 CBC6 cells (ChR2-driven) or natural photostimulation of cones (cone-driven). Example
614 responses to dispersed (top) and clustered spots (bottom) are shown. **f, h**) Responses
615 to dispersed vs. clustered spots in many individual non-alpha On-RGCs. With both
616 optogenetic and natural stimulation, the clustered spots elicited larger EPSCs than did
617 the dispersed spots (ChR2-driven: dispersed=196 ± 19 pA, clustered=553 ± 60 pA,
618 n=11 each; p<0.0001; paired t-test. Cone-driven: dispersed=280 ± 19 pA,
619 clustered=615 ± 59 pA, n=17 each; p<0.0001; paired t-test). For both stimulation
620 protocols, TTX reduced EPSCs from clustered spots, eliminating the preference for
621 clustering (ChR2-driven: dispersed=191 ± 17 pA, clustered=191 ± 17 pA, n=12 each;
622 p=0.9876, paired t-test. Cone-driven: dispersed=239 ± 15 pA, clustered=242 ± 16 pA,
623 n=17 each; p=0.8555, paired t-test). Filled black circles and error bars are mean ± sem.
624 **g, i)** Summary results showing that the preference for clustering is eliminated by
625 blocking NaV channels with TTX. **g)** For ChR2-driven responses without TTX, 11 out
626 of 12 cells had a >50% preference for clustered stimulation (defined as >50% larger
627 EPSCs), but with TTX, 0 out of 12 cells had a >50% preference for clustered
628 stimulation. **i)** For cone-driven responses without TTX, 13 out of 17 cells had a >50%
629 preference for clustered spots, but with TTX only one cell preferred clustering. Note
630 that natural photo-stimuli were delivered in mesopic background with 100% contrast.
631 The duration of stimuli was 10 ms in all experiments.

632 We recorded EPSCs in these non-alpha On-RGCs, elicited either by optogenetically
633 photo-stimulating CBC6 cells or by naturally stimulating cone photoreceptors (Fig 8 b-
634 c). We found that the majority of non-alpha RGCs responded preferentially to the
635 clustered stimuli in both sets of experiments, and this preference was abolished by
636 TTX (Fig 8 d-i). Together, these data indicate that NaV channel mediated amplification
637 from A2 cells is a common feature of inner retinal circuitry, accentuating representation
638 of spatial proximity in many types of On-RGCs in a previously unappreciated manner.

639 **DISCUSSION**

640 **Amacrine cell-mediated amplification of bipolar cell synaptic transmission**

641 A2 amacrine cells are the crucial hub in the retina where signals from rods and cones
642 merge to influence the firing of RGCs. In mammalian retinas, about 20–50 rods
643 converge upon each RBC, 20–25 RBCs converge upon each A2 amacrine cell, and 6-
644 10 A2 cells, via their connection with On-CBC terminals, drive each On-alpha RGC.
645 Overall, signals from >10000 rods converge upon a single ganglion cell[17,47-49]. The high
646 degree of convergence increases the amplitude of rod-driven light responses, while
647 non-linear properties of the rod synapse diminish responses triggered by uncorrelated
648 events, increasing signal to noise[50-52].

649 The cone pathway, in contrast, exhibits much less convergence. Each cone bipolar cell
650 receives input from 2-6 cones[39], and each RGC receives input from <400 cone bipolar
651 cells[20]. In dim (mesopic) light, where cones are just beginning to respond and rods are
652 nearing saturation[43,53], bipolar cell light responses are small, hampering detection
653 above noise. Our results indicate that NaV-mediated excitability of A2 amacrine cells,
654 communicated to On-CBCs through gap junctions, amplifies chemical synaptic
655 transmission from On-CBCs to On-RGCs, which should improve detection of cone-
656 driven signals. With weak stimulation of CBC6 cells, A2 cell-mediated amplification is
657 profound, increasing the amplitude of EPSCs by as much as 5-fold (Fig. 2h). In
658 contrast, amplification of responses to stronger stimuli is more modest, increasing
659 EPSCs by roughly 20% or not at all. This suggests that amplification is restricted largely
660 to mesopic background, where it is needed to improve stimulus detection, in contrast
661 to photopic light, where amplification is unnecessary. In scotopic light, where rods
662 rather than cones are generating light responses, A2 amplification of RGC synaptic
663 input is also absent[17].

664 **The role of electrical excitability**

665 A2 cells were previously found to slightly accelerate On-CBC to RGC synaptic
666 transmission[17] but our findings reveal a previously unappreciated function of electrical
667 excitability in CBC6 cells, amplifying spatially adjacent signals independent of the
668 position within the RGC receptive field where they are displayed. This capability
669 resembles the sophisticated response properties of complex cells in the primary visual

670 cortex[54], many synapses further along in the visual pathway. In cortical complex cells,
671 shape detection agnostic to position emerges from the hierarchical nature of the visual
672 pathway, involving many processing steps with each set of neurons converging on a
673 smaller set in each successive steps[55,56]. But here, only 2 synapses into the visual
674 system, similar feature detection properties emerge, which can be explained by the
675 thresholding property of electrical excitability. This accentuates spatially correlated
676 stimuli from neighboring presynaptic bipolar cells. Amplification only occurs if there are
677 enough convergent inputs to bring the A2 cell to spike threshold, accounting for the
678 preference for spatially clustered stimuli.

679 While our study focused on A2 amacrine cells, other narrow-field amacrine cell types,
680 including the A8 amacrine cell, also has electrical synapses on type 6 bipolar cells[57].
681 Likewise, several other types of On-CBCs are also electrically coupled to A2 amacrine
682 cells, including the type 5a and 7 On-CBCs[21]. Amongst the On-CBCs, type 5a, 6 and
683 7 bipolar cells constitute the majority of gap junctions on A2 cell[21], and like most bipolar
684 cells are devoid of NaV channels (Extended Data Fig. 5). Altogether, these cells
685 comprise of almost 60% of On-CBCs[20], stratify in three inner plexiform layers[58], and
686 likely provide excitatory input to a large fraction of On-RGCs. Consistent with this, our
687 results show that NaV channel-mediated amacrine cell-driven amplification is not
688 exclusive to On-alpha RGCs but applies to many other types of On-RGCs (Fig. 8).
689 Hence the mechanism we have revealed is a common feature of inner retinal circuitry,
690 accentuating spatial proximity in a previously unappreciated manner.

691 It has been suggested that the complex morphology of the A2 axodendritic tree endows
692 the cell with distinct local and global integration capabilities[59]. However, the
693 correspondence of the spatial extent of the axodendritic tree (~36 um wide), and the
694 spatial separation of visual stimuli that recruits NaV-mediated excitability (2 bars within
695 ~36 um; Fig. 5h), suggests that information integrated over the entire cell governs
696 amplification of CBC6 cell output. Our findings hint at the function of the single “blind
697 alley” appendage protruding from the soma of the A2 cells, which contains a high
698 density of NaV channels, reminiscent of an axon initial segment[60]. In many brain
699 neurons, spikes can be initiated independently in multiple dendritic branches, each
700 comprising a computational unit that pre-processes synaptic inputs[61]. These dendritic

701 spikes spread to the axon initial segment, which generates all-or none spikes that
702 control neuronal output.

703 In A2 amacrine cells, the single central NaV channel-containing appendage suggests
704 that the A2 cell comprises a single “computational unit”, at least under the experimental
705 conditions used in this study. In this scenario, synaptic inputs that are spatially
706 distributed across the dendritic tree of an A2 cell are integrated in one central location
707 near the soma, which generates NaV-mediated spikes that back-propagate throughout
708 the axodendritic tree. Presumably, these spikes reach chemical synaptic outputs onto
709 Off-CBCs and electrical synapses onto On-CBCs, in both cases amplifying synaptic
710 output.

711 **The role of gap junctions**

712 We found that A2-mediated amplification depends critically on gap junctions that
713 electrically couple CBC6 cells and A2 cells, which are located where fine processes of
714 A2 cells intersect with synaptic terminals of CBC6 cells[29]. Pharmacological uncoupling
715 of gap junctions with MFA had two dramatic effects on the physiology of CBC6 cells.
716 First, uncoupling increased the input resistance of the CBC6 cell, such that small
717 membrane currents resulted in much larger changes in membrane potential, as noted
718 previously[37,62]. This leads to an increase in calcium-dependent neurotransmitter
719 release, increasing the gain of synaptic transmission to RGCs (Fig. 2h). Second,
720 uncoupling gap junctions removed NaV-mediated amplification of CBC6 synaptic
721 transmission, decreasing the gain of CBC6 to RGC synaptic transmission.
722 Interestingly, these two effects tend to offset one another, at least under our
723 experimental conditions. Without the boost provided by the A2 amplifier, synaptic gain
724 of the CBC6 output synapse would be low, shunting voltage changes in CBC6
725 terminals and reducing transmission. The rod pathway is highly convergent, such that
726 many rods synapse onto far fewer rod bipolar cells (RBCs) and many RBCs synapse
727 onto still fewer A2 amacrine cells, aiding in signal amplification. But the cone pathway
728 exhibits much less convergence, making the A2 amplifier especially important for
729 downstream signal detection.

730 Under natural conditions, the gap junctional coupling between A2 and On-CBCs is
731 variable, subject to regulation by the neuromodulators dopamine and nitric oxide (NO)

732 leading to uncoupling of gap juctions[63,64]. Dopamine and NO are released from distinct
733 classes of amacrine cells whose activity is regulated by background illumination[65,66].
734 In bright background light or photopic conditions, dopamine and NO release is high,
735 and gap junctions are uncoupled. This makes intuitive sense, as signaling through the
736 cone pathway is strong in photopic light, making A2-mediated amplification
737 unnecessary. In very dim background light or scotopic conditions, rods are active, but
738 the rod pathway is not subject to A2-dependent amplification because A2 cells and
739 RBCs are not electrically coupled. Under photopic conditions, A2-dependent
740 amplification should be minimized by dopamine-dependent uncoupling of A2 cells from
741 On-CBCs[40]. Hence, we expect that the A2 amplifier will have the greatest effect under
742 mesopic conditions, when rod signaling is saturated but cones are barely exceeding
743 threshold for responding to light[43]. It is precisely in this situation where amplification
744 through the cone pathway should be most important for signal detection by
745 downstream circuitry. Rod photoreceptors and rod bipolar cells are absent from
746 primate fovea[67], which may make amplification through this pathway particularly
747 important for human mesopic vision.

748 Synaptic amplification by gap junctional-mediated sharing of excitability may be a
749 common phenomenon. In the auditory brainstem, excitatory neurons can augment the
750 electrical excitability of gap junction-coupled inhibitory interneurons[68]. Likewise, in the
751 spinal cord, inhibitory interneurons can enhance synaptic output of electrically-coupled
752 excitatory neurons[69]. Throughout the nervous system, gap junctions and chemical
753 synapses co-exist and work in concert to influence the output of excitatory cells[70-72].
754 Gap junctional sharing of excitability among inhibitory interneurons promotes temporal
755 coincidence detection[73]. Our findings suggest that sharing of excitability via gap
756 junctions can also promote detection of spatial continuity to enhance object recognition
757 by the visual system.

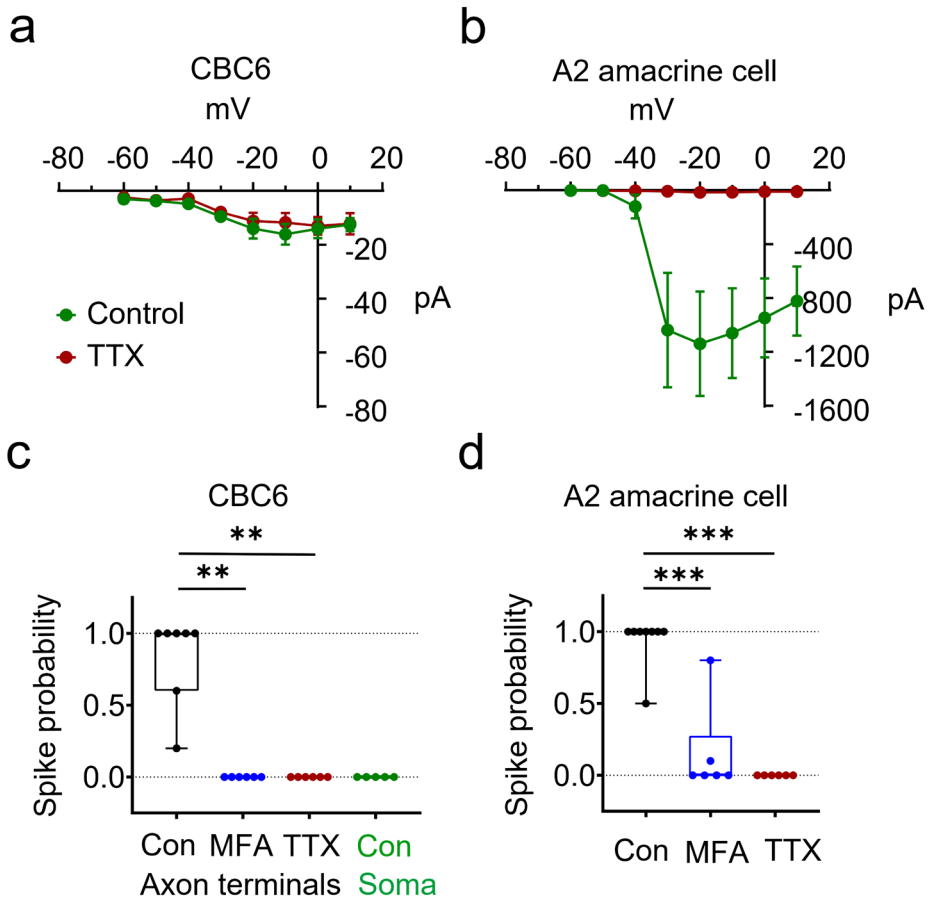

Extended Data Figure 1. NaV-mediated excitability of A2 amacrine cells but not CBC6 cells. a, b) Current vs. voltage curves for peak inward current in CBC6s and A2 amacrine cells before and after addition of 1 μM TTX. At all voltage steps tested, TTX-inhibited NaV current in A2 cells was significantly larger than in CBC6 cells (two-way ANOVA: CBC6 cells, treatment × voltage steps, $F(1,12)=0.1945$, $p=0.7559$; treatment, $F(1,8)=0.4910$, $p= 0.5034$, n=5 each; A2 cells, treatment × voltage steps, $F(1, 10)=7.495$, $p=0.0182$; treatment, $F(1,8)=8.729$, $p= 0.0183$, n=5 each). **c)** Group data showing spike probability of CBC6 somata (0.00 ± 0.00, n=5) and CBC6 axon terminals in control, and after MFA or TTX (control=0.82 ± 0.11, n=7, MFA=0.00 ± 0.00, n=6, TTX=0.00 ± 0.00, n=6). Note that the probability of spiking in the CBC6 cell terminals was abolished by MFA or TTX application (Kruskal-Wallis test, $p<0.0001$; control vs. MFA, $p=0.0012$; control vs. TTX, $p=0.0012$; Mann-Whitney test). **d)** Spike probability of A2 cells in control, and after MFA and TTX (control: 0.93 ± 0.06, n=8; MFA: 0.15 ± 0.13, n=6; TTX: 0.00 ± 0.00, n=6). Note that the probability of spiking in the A2 cells declined significantly after MFA treatment and was completely abolished by TTX (Kruskal-Wallis test, $p<0.0001$; control vs. MFA, $p=0.0007$; control vs. TTX, $p=0.0003$; Mann-Whitney test). CBC6 cells expressed ChR2 and light flash intensity of 0.24

775 mW/cm^2 and 10 ms duration were used to optogenetically stimulate these cells**.** Spike
776 probability denotes the fraction of stimulus that elicited spikes, which could range from
777 0 to 1. Box plots depict median, min and max values. Data in a, b are mean ± sem.

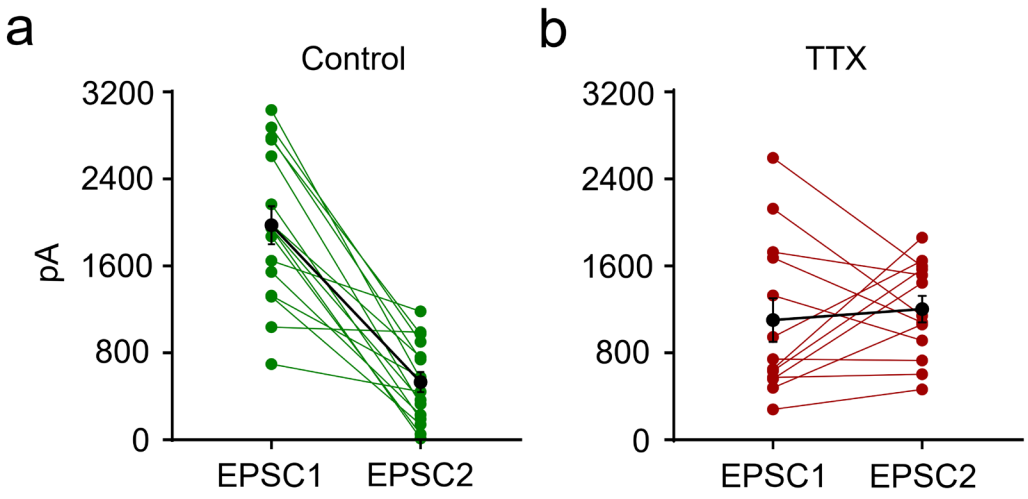

778 **Extended Data Figure 2. TTX changes short-term synaptic plasticity (paired-**
779 **pulse behavior) from depressing to not depressing at the CBC6 cell to On-alpha**
780 **RGC synapse. a, b)** EPSCs elicited by two optogenetic stimuli (2ms light flashes) with
781 an inter-stimulus interval of 50 ms before (a) and after (b) adding TTX (1 μM). Green
782 and red points and lines represent individual recordings, black points and lines
783 represent mean ± sem values. Note that paired EPSCs decremented without TTX, but
784 grew in amplitude with TTX (control, n=16, TTX, n=13).

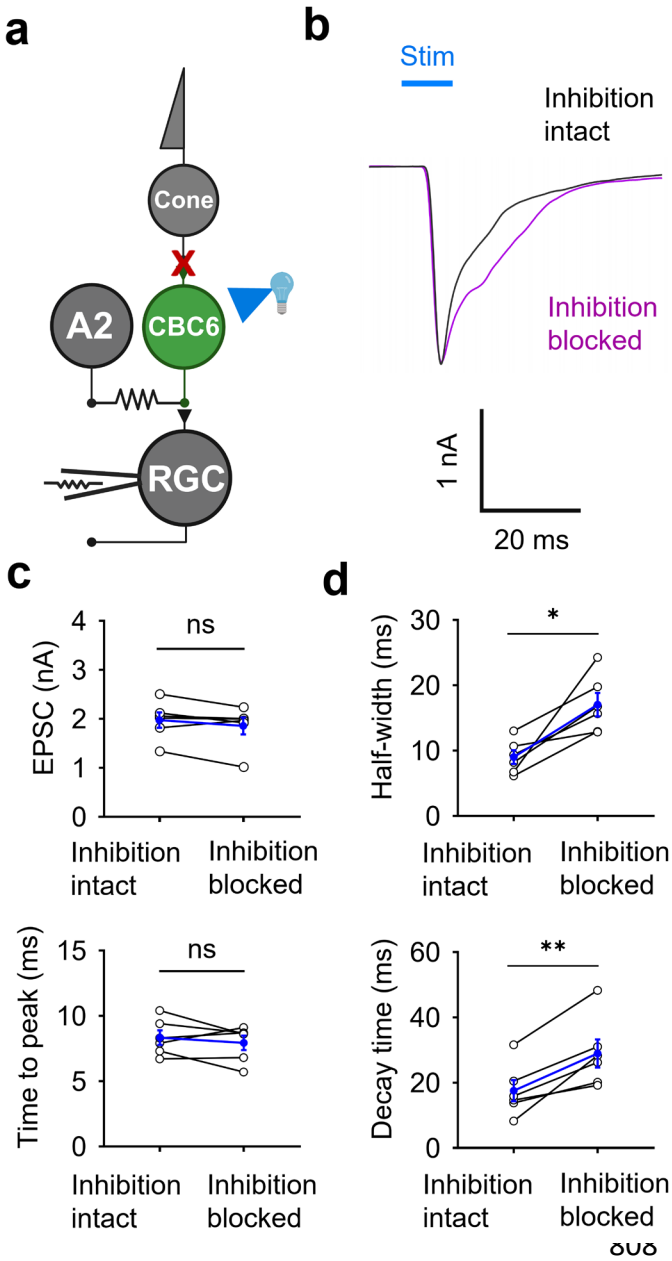

Extended Data Figure 3. Inhibition does not alter the amplitude or time to peak EPSC. a) Retinal circuit diagram showing the experimental arrangement. Full-field light flashes at an intensity of 8.01 mW/cm^2 were used to optogenetically stimulate CBC6 cells and whole-cell patch clamp recordings were obtained from On-alpha RGCs to measure evoked EPSCs under voltage-clamp. **b)** Example EPSCs recorded from On-alpha RGCs with inhibition intact (black) and blocked (magenta). Inhibition was blocked with antagonists of GABAa receptors (gabazine), GABAc receptors (TPMPA) and glycine receptors (strychnine). **c)** Inhibitory receptor blockers did not significantly alter the peak amplitude of EPSCs (inhibition intact=1.97 ± 0.15 nA, inhibition blocked=1.85 ± 0.17 nA, n=6 each; p=0.1562, Wilcoxon signed rank test) not did it affect time to peak (inhibition intact=8.33 ± 0.55 ms, inhibition blocked=7.93 ± 0.55 ms; p=0.4435, paired t-test). **d)** However, blocking inhibition prolonged EPSCs in every recording, both in terms of their half-width (inhibition intact=9.01 ± 1.05 ms, inhibition blocked=17.02 ± 1.78 ms; p=0.0122, paired t-test) and their 90%-20% decay time (inhibition intact=17.46 ± 3.25, inhibition blocked=28.86 ± 4.30 ms; p=0.0053, paired t-test). Blue circles and error bars indicate mean ± sem. Prolonged half-width and decay time suggests a delayed contribution of a non-A2 amacrine cell (presumably wf-Acs) in shaping the output from CBC6 cells.

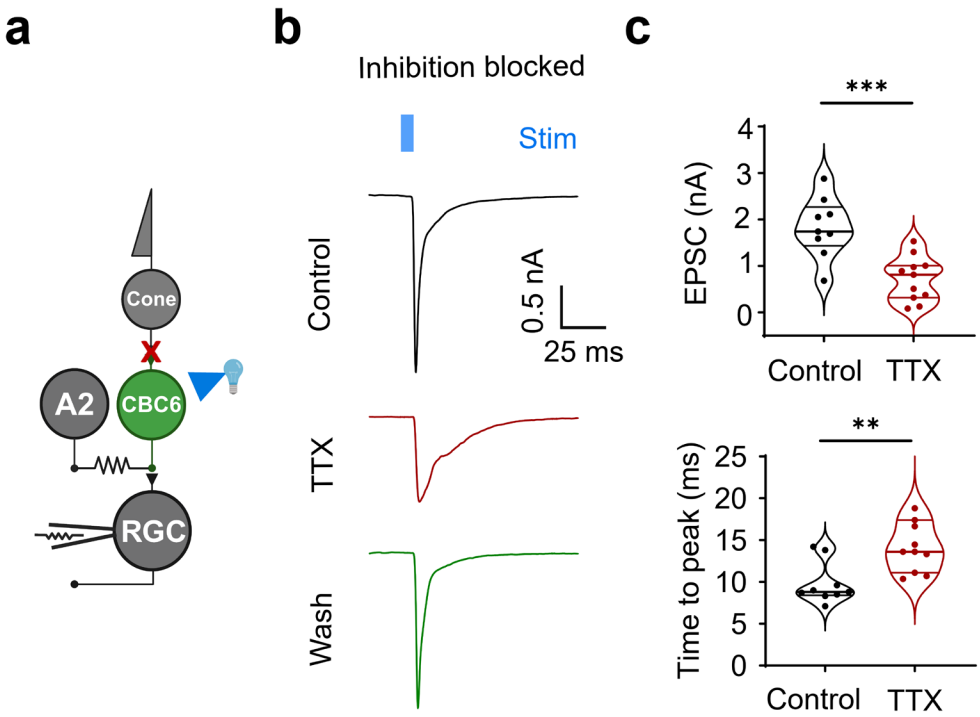

818 **Extended Data Figure 4. TTX reduces the amplitude and prolongs the time to**
819 **peak of EPSCs even in the absence of inhibition. a)** Retinal circuit diagram showing
820 the experimental arrangement. Full-field light flashes at an intensity of 8.01 mW/cm^2
821 were used to optogenetically stimulate CBC6 cells and whole-cell patch clamp
822 recordings were obtained from On-alpha RGCs to measure evoked EPSCs under
823 voltage clamp. **b)** Example EPSCs recorded from On-alpha RGCs in the absence (top
824 and bottom) and the presence of 1 μM TTX (middle). Inhibition was blocked throughout
825 these experiments with antagonists of GABAa (gabazine), GABAc (TPMPA) and
826 glycine receptors (strychnine). **c)** Group data showing that EPSC amplitude and time
827 to peak were altered by TTX, even though inhibition was blocked. TTX significantly
828 reduced the peak amplitude (control=1828 ± 214 pA, n=9; TTX=721 pA ± 159 pA,
829 n=11; p=0.0007; unpaired t-test) and delayed the time to peak (control=9.8 ± 0.8 ms;
830 TTX=16.3 ± 2.4 ms; p=0.0029; Mann-Whitney test).

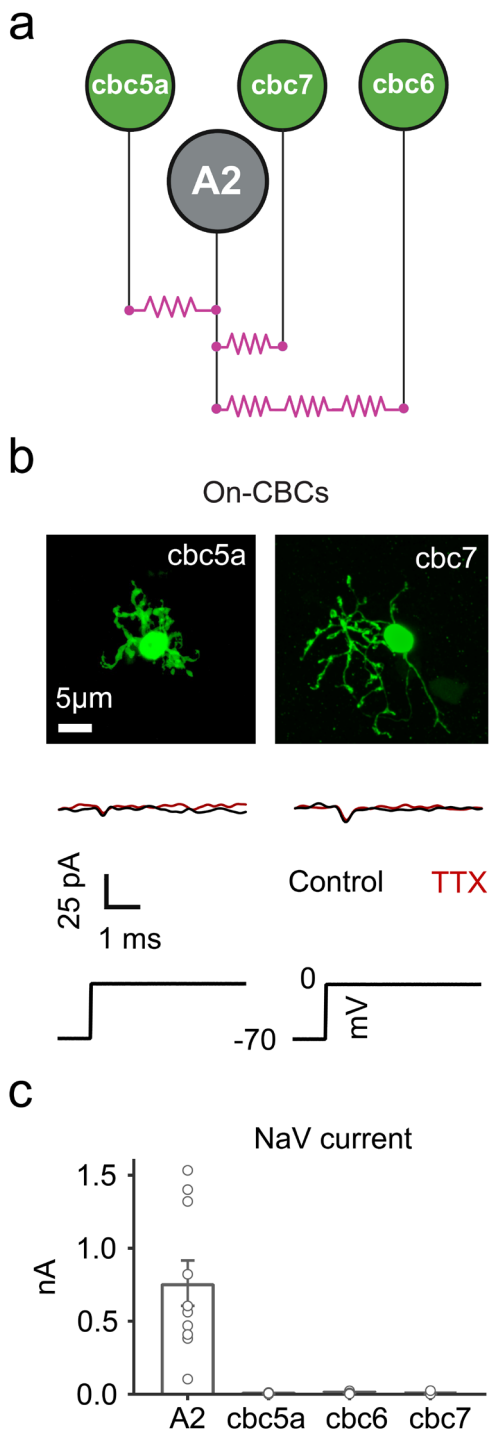

Extended Data Figure 5. Other On-CBCs that are electrically coupled to A2 amacrine cells lack NaV channels. a) Schematic of gap junction circuitry between On-CBCs (green) and A2 amacrine cells. Gap junctions are highlighted in magenta. **b)** Examples of dye-filled On-CBCs in the Kcng4-cre X Ai9 mice; cbc5a (left), cbc7 (right). These cells were identified based on tdTomato expression[19], axonal arbor size and stratification pattern[74]. Under voltage-clamp, cbc5a and cbc7 cells hardly exhibited depolarization-gated inward current (bottom), indicating lack of NaV channels just like their counterpart, cbc6 cells. Note that gap junctions, voltage-gated Ca^{2+} and K^{+} channels were blocked prior to NaV current recordings. **c)** Comparison of depolarization evoked inward or NaV current in A2 cell and its major gap junction partners (A2= 761 ± 155 pA, n=10; cbc5a= 5.2 ± 1.7 pA, n=8; cbc6= 11.3 ± 2.6 pA, n=8; cbc7= 6.4 ± 3.2 pA, n=7). Note that cbc5a and cbc7, together with cbc6 cells constitute almost 60% of On-CBCs[20] and 90% of bipolar cell gap junctions on A2 cell[21], implying that multiple On-subcircuits are subject to A2-driven amplification as shown in Figure 8.

Supplementary information

Contribution of gap junctions to the passive membrane properties of CBC6 cells

By removing NaV-mediated amplification, one might expect that uncoupling CBC6 cells from A2 cells would reduce the amplitude of EPSCs recorded in the RGCs. However, EPSC amplitude either increased or remained unaltered after MFA application (Fig. 2, 3). For example, MFA increased the peak EPSC triggered by 1 ms optogenetic

837 stimulation by almost 2-fold (control=965 ± 159 pA, n=16; MFA=1794 ± 104 pA; n=24;
838 p=0.0002). A previous study showed that gap junctions account for a large fraction of
839 the resting membrane conductance of CBCs[37]. We reasoned that by decreasing the
840 resting conductance, gap junction uncouplers would allow membrane currents elicited
841 by optogenetic stimulation to generate larger voltage changes. This would increase
842 activation of voltage-gated Ca^{2+} channels and increase neurotransmitter release,
843 perhaps enough to offset the loss of the A2 cell amplifier. We tested this idea by
844 applying voltage steps to CBC6 cells and found that MFA treatment increased their
845 input resistance (control=0.79 ± 0.06 GΩ, n=11; MFA=3.50 ± 0.44 GΩ; n=10;
846 p=0.0002) (Supplementary Fig. 1a, b). Consistent with this, optogenetic stimuli
847 generated a much larger depolarization of CBC6 cells after MFA treatment (control=
848 4.14 ± 0.69 mV; MFA=13.50 ± 2.36 mV; n=6 each; p=0.0094) (Supplementary Fig. 2).
849 MFA also increased the input resistance of CBC5A cells (control=0.98 ± 0.09 GΩ,
850 n=11; MFA=4.55 ± 0.69 GΩ; n=8; p=0.0012) (Supplementary Fig. 3), another On-
851 bipolar cell type that forms gap junctions with A2 cells[19]. However, MFA had no effect
852 on the input resistance of rod bipolar cells, which are devoid of gap junctions (control=
853 3.31 ± 0.38 GΩ; MFA=4.17 ± 0.71 GΩ; n=10 each; p= 0.3258) (Supplementary Fig.
854 1c, d).

855 Next, we tested the effect of gap junction uncoupling on synaptic transmission from
856 CBC6 cells. To remove any contribution from NaV channel-mediated amplification,
857 TTX was present throughout these experiments. Under these conditions, 1 ms
858 optogenetic stimulation of CBC6 cells elicited small EPSCs in RGCs, but these grew
859 much larger after treatment with MFA (without MFA=158 ± 39 pA, n=14; MFA=1789 ±
860 116 pA; n=11; p<0.0001) (Supplementary Fig. 1e-g). Another gap-junction uncoupler,
861 18β-glychyrhhetinic acid (18β-GRA) also increased EPSCs in RGCs (Supplementary
862 Fig. 4). However, MFA had no effect on EPSCs elicited in A2 cells upon rod bipolar cell
863 photostimulation (without MFA=427 ± 93 pA, n=11; MFA=434 ± 81 pA; n=10;
864 p=0.8633) (Supplementary Fig. 1h-j).

865 Together, these experiments reveal that gap junctions set the resting membrane
866 resistance of CBC6 cells and other electrically coupled On-CBCs, and that
867 depolarization whether elicited by physiological or optogenetic stimuli, is reduced by
868 this gap junctional shunt. Activation of NaV channels in the A2 cell helps offset this
869 signal reduction, ensuring that depolarization of CBC6 terminals can effectively
870 activate voltage-gated Ca^{2+} channels and trigger neurotransmitter release.

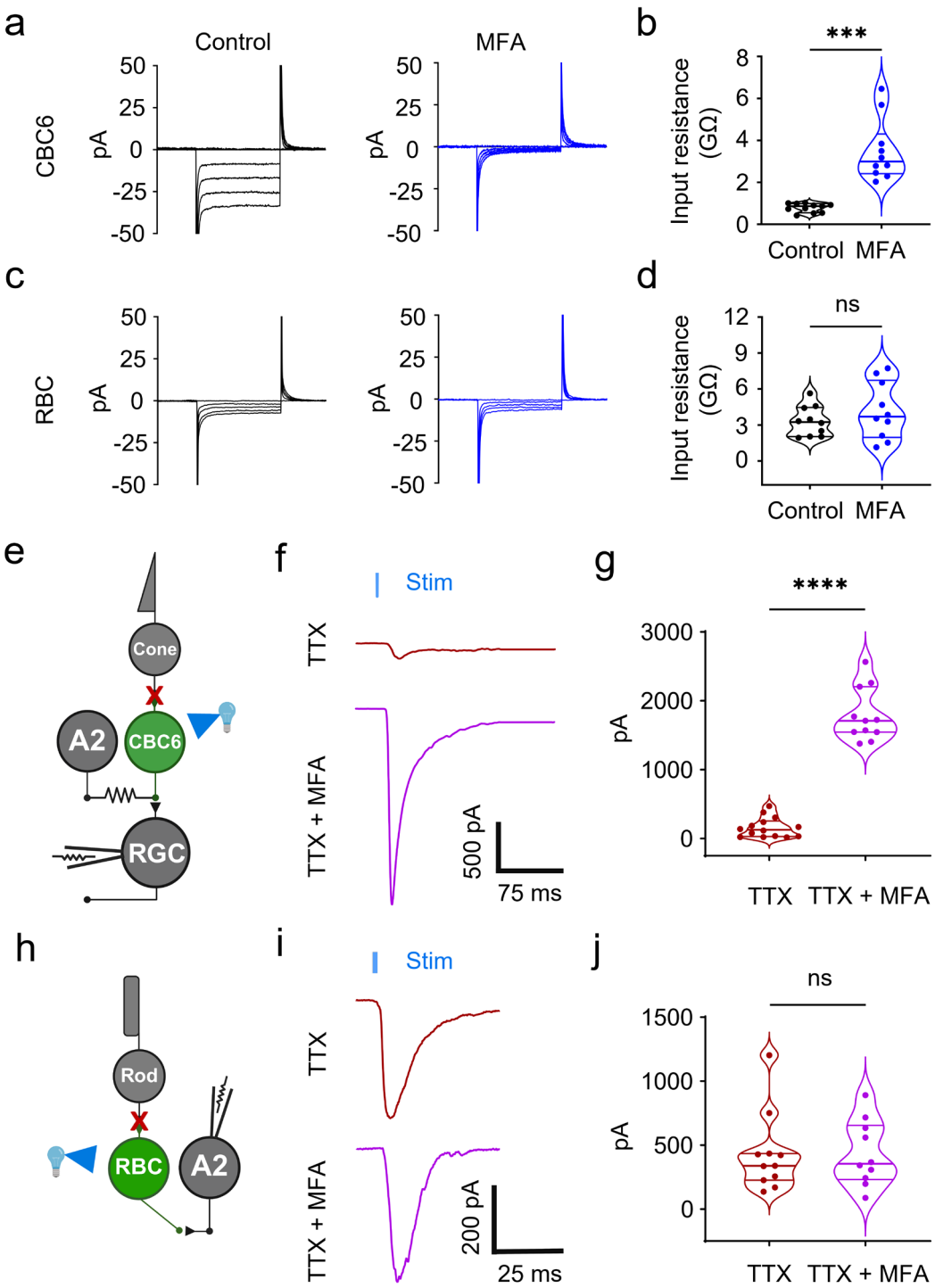

871 **Supplementary Figure 1. Gap junctions determine the input resistance of CBC6**
872 **cells. a-d)** Membrane currents recorded from CBC6 cells (a) and RBCs (c) in response
873 to a series of hyperpolarizing voltage steps (50 msec duration), with and without MFA
874 pre-treatment to uncouple gap junctions. b, d) Steady-state input resistance (ΔV/ΔI),
875 measured over the final 25 msec of the voltage steps. Note that MFA increased input
876 resistance in CBC6 cells (b) but not in RBCs (d). MFA increased the input resistance

877 of CBC6 cells by almost 4-fold (control=0.79 ± 0.06 GΩ, n=11; MFA=3.50 ± 0.44 GΩ;
878 n=10; p=0.0002; unpaired t-test) but had no effect on the input resistance of RBCs
879 (control=3.31 ± 0.38 GΩ; MFA=4.17 ± 0.71 GΩ; n=10 each; p= 0.3258; unpaired t-
880 test). **e-j)** The gap junction shunt reduces synaptic efficacy of the CBC6 output synapse
881 but not the RBC output synapse. **e, h)** Retinal circuit diagrams showing experimental
882 arrangements. CBC6 cells or RBCs were optogenetically stimulated, eliciting EPSCs
883 that were measured in the post-synaptic RGC or A2 cell. In all cases, TTX was present
884 to block the NaV-dependent A2 cell amplifier. EPSCs elicited by stimulating CBC6 cells
885 were enhanced by uncoupling gap junctions with MFA **(f, g)**, whereas EPSCs elicited
886 by stimulating RBCs were unaffected **(h, i).** MFA enhanced CBC6 output by almost 11-
887 fold (before MFA=158 ± 39 pA, n=14; after MFA=1789 ± 116 pA; n=11; p<0.0001;
888 unpaired t-test) but had no effect on RBC output (before MFA=427 ± 93 pA, n=11;
889 MFA=434 ± 81 pA; n=10; p=0.8633; Mann-Whitney test).

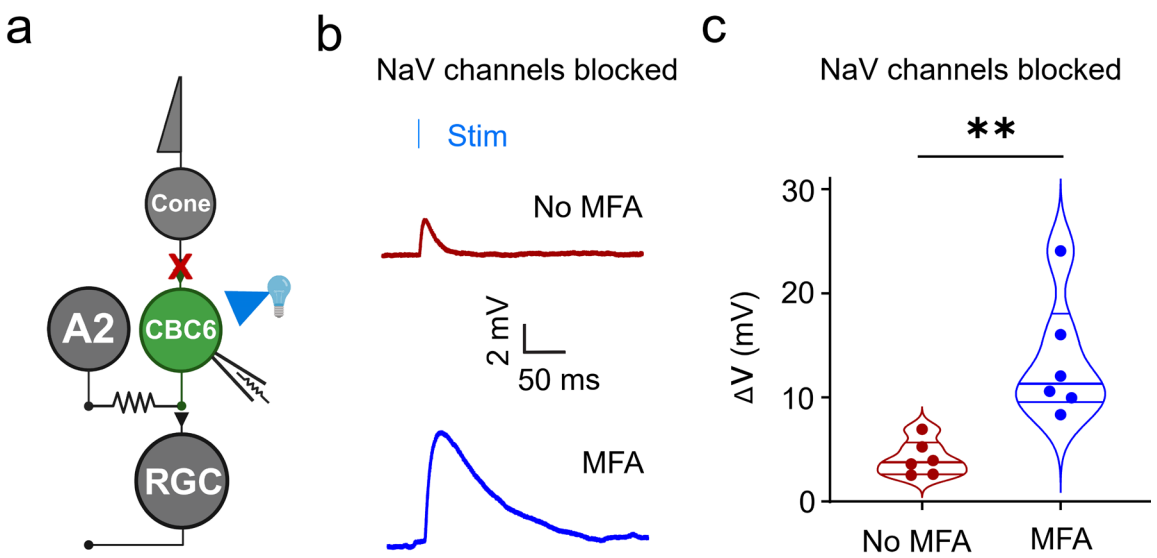

890 **Supplementary Figure 2. Uncoupling gap junctions enhances optogenetically-**
891 **evoked voltage responses in CBC6s. a)** Retinal circuit diagram showing the
892 experimental arrangement. 1 ms full-field light flashes at an intensity of 1.21 mW/cm^2
893 were used to optogenetically stimulate CBC6 cells and whole-cell current clamp
894 recordings were obtained from a CBC6 cell to measure changes in membrane
895 potential. **b)** An example recording from CBC6 cell before (top) and after treatment with
896 MFA (bottom). NaV channels were blocked with TTX prior to recordings. **c)** Group data
897 (violin plot) showing that MFA increases the evoked depolarizations by almost 3-fold

898 (before MFA=4.14 ± 0.68 mV; after MFA=13.50 ± 2.36 mV, n=6 each, p=0.0094,
899 unpaired t-test).

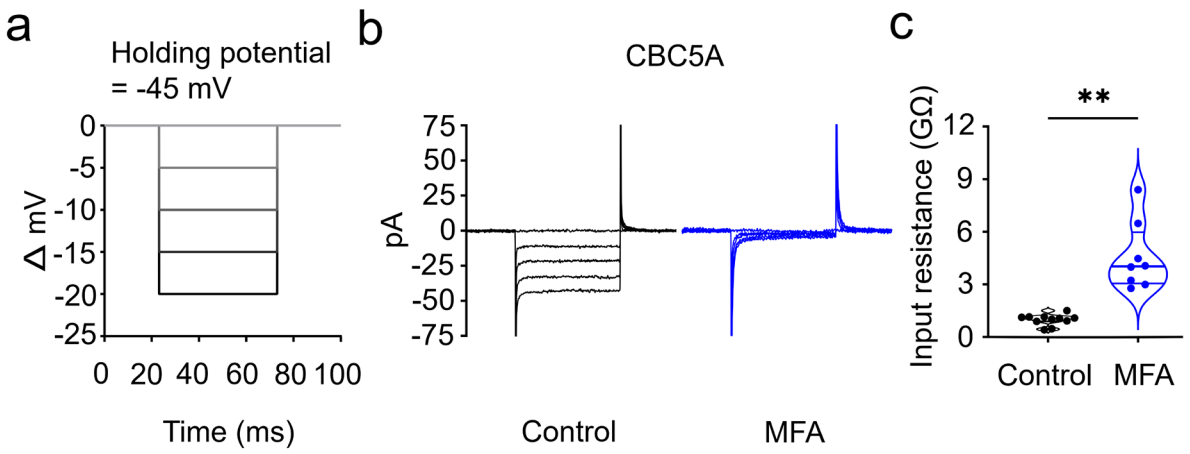

900 **Supplementary Figure 3. Gap junctions determine the input resistance of CBC5A**
901 **cells. a)** Input resistance was measured by delivering a series of hyperpolarizing
902 voltage clamp pulses from -45 mV to -65 mV. **b)** Current responses in CBC5A cells
903 before and after MFA treatment. **c)** Group data (violin plots) showing calculated steady-
904 state input resistance. Note that MFA increased the input resistance of CBC5A cells
905 by almost 4-fold (control=0.98 ± 0.09 GΩ, n=11; MFA=4.55 ± 0.69 GΩ; n=8; p=0.0012;
906 unpaired t-test).

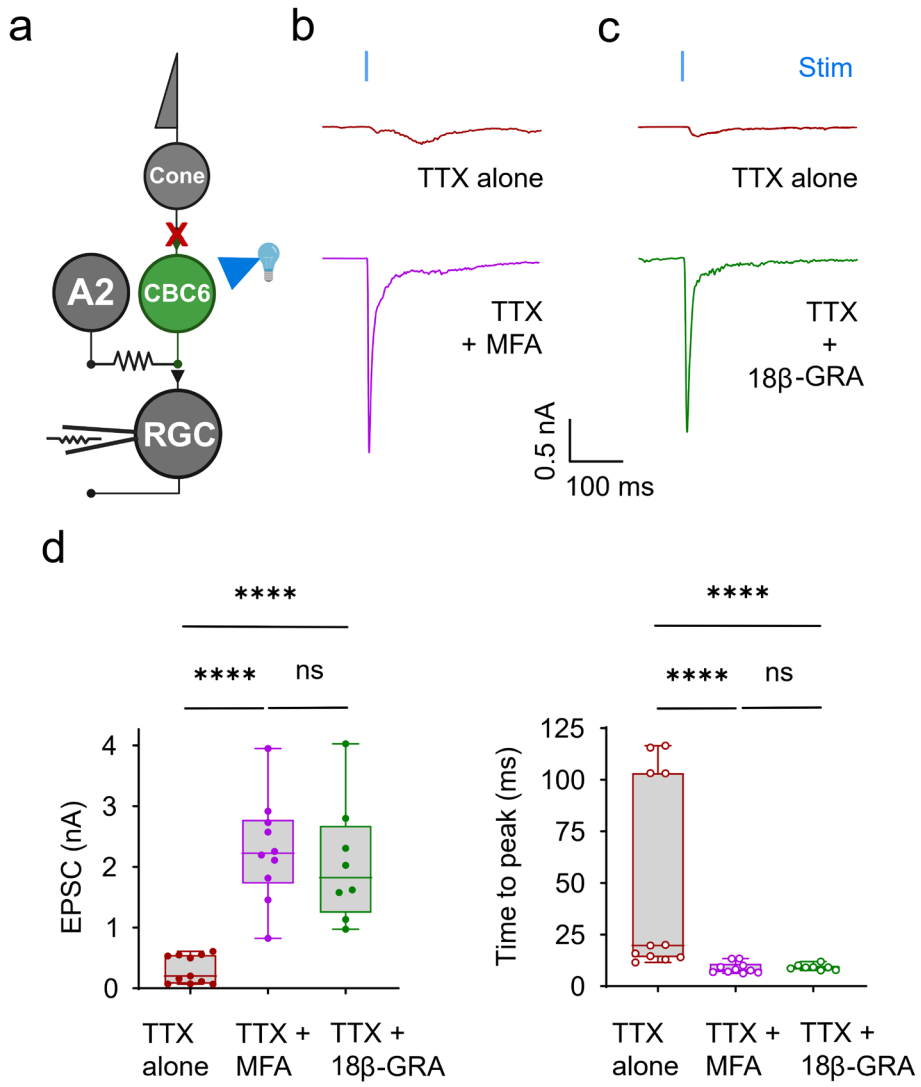

Supplementary Figure 4. Uncoupling gap junctions increases evoked synaptic transmission at the CBC6 to On-alpha RGC synapse without NaV-mediated amplification. a) Retinal circuit diagram showing the experimental arrangement. Full-field light flashes (0.3ms) at an intensity of 8.01 mW/cm^2 were used to optogenetically stimulate CBC6 cells and whole-cell patch clamp recordings were obtained from an RGCs to measure evoked EPSCs under voltage clamp. **b-c)** EPSCs elicited by a single flash were increased in amplitude after uncoupling gap junctions with MFA (**b**) or 18β-GRA (**c**). TTX was present throughout to block NaV-mediated excitability and eliminate A2 cell-mediated amplification. **d)** Group data (box plots) showing peak EPSC amplitude before (TTX alone, n=11), and 45 min after treatment with MFA (n=10) or 18β-GRA (n=8). Note that treatment with either MFA or 18β-GRA dramatically increased peak EPSC amplitude (Kruskal-Wallis test: $p<0.0001$; post-hoc Mann-Whitney test: TTX alone=311 ± 70 pA, MFA=2282 ± 270 pA, 18β-GRA=2057 ± 352 pA; TTX alone vs. MFA, $p<0.0001$; TTX alone vs. 18β-GRA, $p<0.0001$) and shortened

921 the time to peak (Kruskal-Wallis test: p=0.0001; post-hoc Mann-Whitney test: TTX
922 alone=49.7 ± 14.4 ms, MFA=8.8 ± 0.8 ms, 18β-GRA=9.2 ± 0.5 ms; TTX alone vs. MFA,
923 p<0.0001; TTX alone vs. 18β-GRA, p<0.0001).

924 # Methods

925 ## Animals

926 Mice were handled in accordance with protocols approved by the UC Berkeley
927 Institutional Animal Care and Use Committee (AUP-2016-04-8700-1) and conformed
928 to the NIH Guide for the Care and Use of Laboratory Animals. CCK-ires-Cre knock-in
929 mice or CCK-Cre mice (Jackson 012706) were used to drive Cre recombinase under
930 the cholecystokinin promoter to label CBC6 cells. BAC-Pcp2-IRES-Cre or Pcp2-cre
931 mice (Jackson 012706) were used to drive Cre recombinase under the control of
932 mouse purkinje cell protein promoter to label RBC cells. Ai32 mice (Jackson 024109)
933 were used to drive channelrhodopsin-2 or eYFP fusion protein in Cre-expressing CBC6
934 or RBC cells. The CCK-Cre, Pcp2-cre and Ai32 alleles were used in the mice in a
935 hemizygous state. Likewise, Kcng4^{-}Cre mice (Jackson: 029414) were crossed with Ai9
936 mice (Jackson: 007909) to drive tdTomato expression in type 5 bipolar cells and alpha
937 RGCs. C57Bl/6J and Kcng4-Cre X Ai9 mice were used to record natural light
938 responses from RGCs. Mice of both sexes were used interchangeably. 2 to 6 months
939 old mice were used for all the experiments.

940 ## Retinal Dissection

941 Mice were euthanized with isoflurane exposure and cervical dislocation. Eyes were
942 enucleated and the retinal dissection was performed in the ACSF (in mM: 119 NaCl,
943 26.2 $NaHCO_3$, 11 Dextrose, 2.5 KCl mM, 1 K_2HPO_4, 1.3 $MgCl_2$* $6H_2O$, 2.5 $CaCl_2$, 293
944 mOsm/Kg). ACSF was oxygenated (5% CO_2, 95% O_2) whenever used. The dissection
945 was performed in room light conditions as described previously[76,77]. In order to record
946 natural light responses from RGCs, the mice were dark adapted overnight. However,
947 dissecting in photopic conditions presumably bleached photoreceptors. Therefore,
948 RGC recordings were performed after a recovery time of 3 hours. For retinal whole-
949 mount experiments, retinas were flattened with 4 relieving cuts. For retinal slice
950 experiments, flattened retinas were mounted on 13 mm diameter 0.45 µm filter paper
951 discs (MF-Millipore) and sliced to a thickness of either 200 or 300 µm with a Stoelting

952 Tissue Slicer. Retinal slices were rotated 90 degrees and mounted within a vacuum
953 grease well.

954 **Electrophysiology**

955 The majority of experiments were performed in the whole-mount retinas. For these
956 experiments, the isolated retinas were incubated in the ACSF containing hyaluronidase
957 (9,800 U/mL) and collagenase (2,500 U/mL) for 15 minutes to facilitate penetration of
958 the inner limiting membrane[78]. Retinas were mounted ganglion cell side up in a
959 recording chamber and held in place with a harp (Warner Instruments). The retinas
960 were continuously superfused with oxygenated (5% CO_2, 95% O_2) ACSF at a flow rate
961 of 4 ml/minute at 33-34 degree Celsius. Reagents for ACSF were purchased from
962 Thermo Fisher Scientific. The cells of interest were viewed under DIC optics or
963 epifluorescence with an upright microscope (Olympus). A2 amacrine cells were
964 identified with the help of DIC optics and/or mCherry expression. RBC and CBC6 cells
965 were targeted with the help of eYFP expression. CBC5A cells were identified with the
966 help of tdTomato expression. Alpha and non-alpha On-RGCs were targeted under DIC
967 optics for optogenetic experiments. For recording natural light responses, On-alpha
968 RGCs were identified with the help of tdTomato expression[46].

969 NaV-currents (Fig. 1) and EPSC recordings (Supplementary Fig. 1) from A2 cells and
970 paired cell experiments (Fig. 3) were conducted in retinal slices. NaV currents and
971 optogenetically evoked-EPSCs from A2 cells were recorded in 300 µm thick slices. For
972 the paired cell experiments, slightly thinner 200 µm retinal slices were used. Superficial
973 layers were avoided and deeply-seated somata (>75 µm) were targeted for patch-
974 clamp recordings or sharp-electrode injections. For A2 cell recordings, the slices were
975 superfused at a rate of 4 ml/ minute at 33-34 degree Celsius, same as for the whole-
976 mount retinas. However, for the paired cell experiments from A2 cells and RGCs (Fig.
977 3), the ACSF flow rate was 6 ml/ minute, which was maintained at 30 degrees Celsius.
978 A slightly faster flow rate and lower temperature somehow enhanced the viability of
979 On-alpha RGCs in the slices.

980 Electrodes were made with borosilicate capillary glass tubing with OD= 1.5 mm, ID=
981 1.17 mm (Warner G150TF-4). For RGC recordings, glass was pulled to a resistance of
982 3-5 MΩs using a Narishige pipette puller. For A2 and BC cell recordings, electrodes
983 used typically had a resistance of 6-8 MΩs and 9-12 MΩs, respectively. For QX-314

984 injections into A2 cells, sharp electrodes with resistance of 40-50 MΩs were used.
985 These pipettes or sharp electrodes were pulled with Sutter Instruments P1000.

986 For voltage clamp experiments, the pipette solution contained (in mM): 123 Cs
987 gluconate, 8 NaCl, 1 $CaCl_2$, 10 EGTA, 10 HEPES, 10 glucose, 5 Mg^{2+} ATP, 5 QX 314,
988 0.01 Alexa 594, pH 7.4 with CsOH, 293 mOsm/Kg. For current clamp experiments, the
989 pipette solution contained (in mM): 125 K^+ Gluconate, 10 EGTA, 10 KCl, 10 HEPES, 4
990 Mg^{2+} ATP, 0.01 Alexa 488 or 594, 293 mOsm/Kg. Alexa Fluor 488, 568 or 594
991 Hydrazide (ThermoFisher Scientific) at 10 μM was used to dye fill cells during recording
992 for confirmation of cell identity. In some cases, 0.2% Neurobiotin was included in the
993 recording pipette to confirm the identity of the cells post-hoc with immunostainings.
994 Whole-cell recordings were sampled at 10 or 20 kHz and filtered at 2 kHz with a
995 Multiclamp 700B amplifier, digitized with a 1440a or 1550a Digidata A-D converter and
996 analyzed offline with Clampfit. Recordings with series resistance with values higher
997 than 10% of the cell membrane resistance or 30 mΩ were discarded.

998 **Pharmacology or drugs used**

999 In all the optogenetic experiments, the kainate receptor antagonist ACET (1 μM) and
1000 the mGluR6 agonist L-AP4 (10 μM) were added to the ACSF in order to block
1001 photoreceptor driven light responses. In addition, NMDA and acetylcholine receptors
1002 were blocked with D-AP5 (50 μM) and Curare (25 μM) respectively. Gabazine (10 μM),
1003 TPMPA (50 μM) and strychnine (10 μM) were added to the ACSF to block ionotropic
1004 $GABA_A$, GABAc and glycine receptors when necessary (Extended Data Fig. 3, 4).
1005 Mibefradil (10 μM) and Nimodipine (10 μM) were used to block voltage-gated calcium
1006 channels (Fig. 1, Extended Data Fig. 1, 5). MFA (100 μM) and 18β-GRA (50 μM) was
1007 used to uncouple gap junctions. TTX (1 μM) was used to block voltage-gated sodium
1008 channels. In addition, QX-314 (5mM) was always included in the pipette while
1009 recording EPSCs from the RGCs. QX-314 (1mM) was injected into the A2 cells with
1010 the help of sharp electrodes (Fig. 3). Pharmacological agents were purchased from
1011 Tocris Biosciences.

1012 **Light stimulation or projection**

1013 Optogenetic stimulation of CBC6s and RBCs was provided by a 470 nm LED delivering
1014 a maximum of $2.1X10^8$ photons/s, (Lumencore or CoolLED pE-4000) measured at the
1015 plane of the retina with a spectrophotometer (Thor Labs). When necessary, stimulation

1016 intensity was varied by changing the duration of the stimulus ranging from 0.1 to 10
1017 ms. Thus, the number of photons delivered during the optogenetic stimulus ranged
1018 from 2.1 X 10^5 (0.1ms or 1%) to 2.1 X 10^7 (10ms or 100%). For optogenetic
1019 experiments in Fig. 4-5, 10 ms stimulus delivered 1 X 10^5 photons/s.

1020 For experiments in Fig. 4-8, bars or spots of light were generated with a Texas
1021 Instruments Digital Light Projector (CEL1015 Light Engine, Digital Light Innovations)
1022 controlled with CELconductor Control Software. Projection of bars or spots of light and
1023 simultaneous EPSCs or spike recordings were controlled by Digidata. All stimuli were
1024 provided through 40X or 60X Olympus objectives except when measuring natural light
1025 responses. In this case, 20X Olympus objective was used to map the entire dendritic
1026 tree of On-alpha RGCs with nine sets of dispersed or clustered spots. For these
1027 experiments, three different stimulus intensities were used: 3.92 X 10^3, 1.98 X 10^4 and
1028 9.92 X 10^4 photons/μm^2/s. The respective background light intensities were: 1.96 X
1029 10^3, 9.92 X 10^3 and 4.96 X 10^4 photons/μm^2/s. Light intensities were converted into
1030 R*/rods/s as described previously[79]. In each case, the contrast was 100%, which was
1031 calculated as follows: Contrast=(Stimulus intensity-Background intensity)/Background
1032 intensity.

1033 **Viral injections**

1034 AAV-PHP.eB-HKamac-mCherry-T2A-TRPV1.PHP.e (10^{13} viral genome particles/mL)
1035 was produced in the Gene Delivery module of the Vision Science Core at UC Berkeley.
1036 Ocular injection of this construct resulted into expression of mCherry specifically in A2
1037 amacrine cells as HKamac is a A2 cell-specific promoter[80]. We injected this viral
1038 construct into the eyes of Cck-Cre-Ai32 mice in order to target A2 cells. In short, mice
1039 were anesthetized with isoflurane. A small hole was made at the margin of the cornea
1040 and sclera by using a 30-gauge needle. Approximately, 1.5 µL of the virus was
1041 intravitreally injected into the eyes of the mice. After injection, mice were returned to
1042 their home cage and monitored, until fully recovered. Retinas were used for
1043 experiments three to four weeks after the injections.

1044 **Immunohistochemistry and scanning**

1045 The dye and/or Neurobiotin injected retinas were fixed with 4% PFA. After washing
1046 steps, they were incubated with Alexa488 or 647 conjugated Streptavidin (S32354 or
1047 S32357, Thermo Fisher Scientific) as described before[81]. Images were scanned with
1048 40X/1.4 oil objective using Zeiss LSM780 Laser Scanning Confocal Microscope. The

1049 z-stacks were acquired at a pixel size of 60 nm X 60 nm at a z-step of 0.3 µm or 1 µm.
1050 In some cases, images captured were deconvolved with Huygens Essential Software
1051 (Scientific Volume Imaging, Netherlands) as described before[82].

1052 **Data Visualization and Statistics**

1053 All reported statistics and figures were generated with GraphPad Prism9. Retinal and
1054 experimental diagrams were created with Biorender.com. Data are presented as mean
1055 ± sem; median and 25th and 75th quartiles; median, minimum and maximum. Normality
1056 was checked with Shapiro-Wilk test prior to applying statistical tests. Significance of
1057 non-normal data was tested with Mann-Whitney U test, Wilcoxon matched-pairs signed
1058 rank test and Kruskal-Wallis test, depending upon the suitability of the tests.
1059 Significance of normal data was examined with unpaired t-test, paired t-test, one-way
1060 ANOVA and two-way ANOVA (generalized linear mixed model) as required. Welch's
1061 correction was applied to unpaired t-tests. Two-way ANOVA was always carried out
1062 with Geisser-Greenhouse correction. F values were rounded up to the closest integer.
1063 In the texts and figure legends, mean ± sem values are reported. Unless mentioned
1064 otherwise, the reported 'n' refers to the number of cells recorded from. Statistical
1065 significance notation were as follows: ns, $p > 0.05$; *, $p= \leq 0.05$; **, $p= \leq 0.01$; ***, $p= \leq$
1066 0.001; ****, $p= \leq 0.0001$.

1067 ## References

1068 1. Pan ZH, Hu HJ. Voltage-dependent Na (+) currents in mammalian retinal cone
1069 bipolar cells. J Neurophysiol. 84(5):2564-71 (2000).
1070 2. Ma YP, Cui J, Pan ZH. Heterogeneous expression of voltage-dependent Na+
1071 and K+ channels in mammalian retinal bipolar cells. Vis Neurosci. 22:119–
1072 133 (2005).
1073 3. Cui J, Pan ZH. Two types of cone bipolar cells express voltage-gated Na+ channels
1074 in the rat retina. Vis Neurosci. 25(5-6):635-45 (2008).
1075 4. Saszik S, DeVries SH. A mammalian retinal bipolar cell uses both graded changes
1076 in membrane voltage and all-or-nothing Na+ spikes to encode light. J Neurosci.
1077 32(1):297-307 (2012).
1078 5. Puthussery T et al. NaV1.1 channels in axon initial segments of bipolar cells
1079 augment input to magnocellular visual pathways in the primate retina. J Neurosci.
1080 33(41):16045-59 (2013).
1081 6. Hellmer CB et al. Morphological and physiological analysis of type-5 and other

1082 bipolar cells in the Mouse Retina. Neuroscience.19, 315:246-58 (2016).
1083 7. Kawai F et al. A subset of cone bipolar cells expresses the Na^+ channel SCN2A in
1084 the human retina. Exp Eye Res. 202:108299 (2021).
1085 8. Ichinose T, Fyk-Kolodziej B, Cohn J. Roles of ON cone bipolar cell subtypes in
1086 temporal coding in the mouse retina. J Neurosci. 34(26):8761-71 (2014).
1087 9. Van Hook MJ, Nawy S, Thoreson WB. Voltage- and calcium-gated ion channels of
1088 neurons in the vertebrate retina. Progress in retinal and eye research. 72:100760
1089 (2019).
1090 10. Cook PB, Werblin FS. Spike initiation and propagation in wide field transient
1091 amacrine cells of the salamander retina. J Neurosci. 14(6):3852-61 (1994).
1092 11. Euler T, Detwiler PB, Denk W. Directionally selective calcium signals in dendrites
1093 of starburst amacrine cells. Nature. 22;418(6900):845-52 (2002).
1094 12. Hausselt SE et al. A dendrite-autonomous mechanism for direction selectivity in
1095 retinal starburst amacrine cells. PLoS Biol. 5(7): e185 (2007).
1096 13. Oesch NW, Taylor WR. Tetrodotoxin-resistant sodium channels contribute to
1097 directional responses in starburst amacrine cells. PLoS One. 27;5(8): e12447
1098 (2010).
1099 14. Vlasits AL et al. A Role for Synaptic Input Distribution in a Dendritic Computation
1100 of Motion Direction in the Retina. Neuron. 89(6):1317-1330 (2016).
1101 15. Wu C et al. Action potential generation at an axon initial segment-like process in
1102 the axonless retinal AII amacrine cell. J Neuroscience. 31:14654-14659 (2011).
1103 16. Bloomfield SA, Völgyi B. Response properties of a unique subtype of wide-field
1104 amacrine cell in the rabbit retina. Vis Neurosci. 24(4):459-69 (2007).
1105 17. Tian M et al. Voltage-gated Na channels in AII amacrine cells accelerate scotopic
1106 light responses mediated by the rod bipolar cell pathway. J Neurosci 30:4650-
1107 4659 (2010).
1108 18. West ER, Cepko CL. Development and diversification of bipolar interneurons in the
1109 mammalian retina. Dev Biol. 481:30-42, (2022).
1110 19. Shekhar K et al. Comprehensive Classification of Retinal Bipolar Neurons by
1111 Single-Cell Transcriptomics. Cell. 166(5):1308-1323.e30 (2016).
1112 20. Helmstaedter M et al. Connectomic reconstruction of the inner plexiform layer in
1113 the mouse retina. Nature. 500(7461):168-74 (2013).
1114 21. Tsukamoto Y, Omi N. Classification of Mouse Retinal Bipolar Cells: Type-Specific
1115 Connectivity with Special Reference to Rod-Driven AII Amacrine Pathways.

1116 Frontiers in neuroanatomy. 11:92 (2017).
1117 22. Schwartz GW et al. The spatial structure of a nonlinear receptive field. Nat Neurosci
1118 15:1572-1580 (2012).
1119 23. Deans MR et al. Connexin36 is essential for transmission of rod-mediated visual
1120 signals in the Mammalian retina. Neuron. 36:703-712 (2002).
1121 24. Baden T, Berens P, Franke K et al. The functional diversity of retinal ganglion cells
1122 in the mouse. Nature. 529, 345–350 (2016).
1123 25. Pan F, Mills SL, Massey SC. Screening of gap junction antagonists on dye coupling
1124 in the rabbit retina. Vis Neurosci. 24: 609 – 618 (2007).
1125 26. Tien NW et al. Homeostatic Plasticity Shapes Cell-Type-Specific Wiring in the
1126 Retina. Neuron. 94:656-665 e654 (2017).
1127 27. Boos R, Schneider H, Wassle H. Voltage- and transmitter-gated currents of all-
1128 amacrine cells in a slice preparation of the rat retina. The Journal of Neuroscience.
1129 13:2874-2888 (1993).
1130 28. Cembrowski MS et al. The mechanisms of repetitive spike generation in an
1131 axonless retinal interneuron. Cell Reports. 1(2):155-66 (2012).
1132 29. Meyer A et al. AII amacrine cells discriminate between heterocellular and
1133 homocellular locations when assembling connexin36-containing gap junctions. J
1134 Cell Sci. 127(Pt 6):1190-202 (2014).
1135 30. Ganzen L, Yadav SC et al. Retinoic Acid-Dependent Loss of Synaptic Output from
1136 Bipolar Cells Impairs Visual Information Processing in Inherited Retinal
1137 Degeneration. J Neurosci. 44(35): e0129242024 (2024).
1138 31. von Gersdorff H, Matthews G. Depletion and replenishment of vesicle pools at a
1139 ribbon-type synaptic terminal. Journal of Neuroscience. 17:1919-1927 (1997).
1140 32. Singer JH et al. Coordinated multivesicular release at a mammalian ribbon
1141 synapse. Nat Neurosci 7:826-833 (2004).
1142 33. Heflin SJ, Cook PB. Narrow and wide field amacrine cells fire action potentials in
1143 response to depolarization and light stimulation. Vis Neurosci. 24(2):197-206
1144 (2007).
1145 34. Park Silvia JH et al. Connectomic analysis reveals an interneuron with an integral
1146 role in the retinal circuit for night vision. eLife. 9: e56077 (2020).
1147 35. Swygart D, Yu WQ, Takeuchi S et al. A presynaptic source drives differing levels
1148 of surround suppression in two mouse retinal ganglion cell types. Nat Commun. 15,
1149 599 (2024).

1150 36. Eggers ED, Lukasiewicz PD. Receptor and transmitter release properties set the
1151 time course of retinal inhibition. J Neurosci 26:9413-9425 (2006).
1152 37. Fournel R et al. Differential Contribution of Gap Junctions to the Membrane
1153 Properties of ON- and OFF-Bipolar Cells of the Rat Retina. Cell Mol Neurobiol.
1154 41(2):229-245 (2021).
1155 38. Fi Jeon CJ, Strettoi E, Masland RH. The major cell populations of the mouse retina.
1156 J Neurosci. 18(21):8936-46 (1998).
1157 39. Behrens C et al. Connectivity map of bipolar cells and photoreceptors in the mouse
1158 retina. eLife. 5: e20041 (2016).
1159 40. Yadav SC, Tetenborg S, Dedek K. Gap Junctions in A8 Amacrine Cells Are Made
1160 of Connexin36 but Are Differently Regulated Than Gap Junctions in AII Amacrine
1161 Cells. Frontiers in molecular neuroscience. 12:99 (2019).
1162 41. Naarendorp F et al. Dark light, rod saturation, and the absolute and incremental
1163 sensitivity of mouse cone vision. J Neurosci. 30(37):12495-507 (2010).
1164 42. Borghuis BG et al. Two-photon imaging of nonlinear glutamate release dynamics
1165 at bipolar cell synapses in the mouse retina. J Neurosci. 33(27):10972-85 (2013).
1166 43. Wang JS, Kefalov VJ. An alternative pathway mediates the mouse and human
1167 cone visual cycle. Current Biology. 19(19):1665-9 (2009).
1168 44. Goetz J et al. “Unified Classification of Mouse Retinal Ganglion Cells Using
1169 Function, Morphology, and Gene Expression.” Cell Reports. 40(2), (2022).
1170 45. Bleckert A et al. Visual space is represented by nonmatching topographies of
1171 distinct mouse retinal ganglion cell types. Curr Biol. 24(3):310-5 (2014).
1172 46. Krieger B, Qiao M, Rousso DL, Sanes JR, Meister M. Four alpha ganglion cell
1173 types in mouse retina: Function, structure, and molecular signatures. PLoS One.
1174 12(7):e0180091 (2007).
1175 47. Tsukamoto Y et al. Microcircuits for night vision in mouse retina. J Neurosci.
1176 21(21):861623 (2001).
1177 48. Volgyi B et al. Convergence and segregation of the interneurons in the mammalian
1178 retina. Neuron. 33:935-946 (2004).
1179 49. Dunn FA et al. Controlling the gain of rod-mediated signals in the Mammalian
1180 retina. J Neuroscience. 26:3959-3970 (2006).
1181 50. Field GD, Rieke F. Nonlinear signal transfer from mouse rods to bipolar cells and
1182 implications for visual sensitivity. Neuron. 34:773-785 (2002).
1183 51. Sampath AP, Rieke F. Selective transmission of single photon responses by

1184 saturation at the rod-to-rod bipolar synapse. Neuron. 41:431-443 (2004)
1185 52. Taylor WR, Smith RG. Transmission of scotopic signals from the rod to rod-bipolar
1186 cell in the mammalian retina. Vision Res. 44(28):3269-76 (2004).
1187 53. Nange Jin et al. Genetic elimination of rod/cone coupling reveals the contribution
1188 of the secondary rod pathway to the retinal output. *Sci. Adv.* 8, eabm4491 (2022).
1189 54. Hubel DH, Wiesel TN. Receptive fields, binocular interaction and functional
1190 architecture in the cat's visual cortex. J Physiol. 160(1):106-54 (1962).
1191 55. Martinez LM, Alonso JM. Construction of complex receptive fields in cat primary
1192 visual cortex. Neuron. 32(3):515-25 (2001).
1193 56. van Kleef JP, Cloherty SL, Ibbotson MR et al. Complex cell receptive fields:
1194 evidence for a hierarchical mechanism. The Journal of Physiology, 588(18), 3457–
1195 3470 (2010).
1196 57. Lee SC et al. Morphology and connectivity of the small bistratified A8 amacrine cell
1197 in the mouse retina. J Comp Neurol. 523(10):1529-47 (2015).
1198 58. Euler T, Haverkamp S, Schubert T, Baden T. Retinal bipolar cells: elementary
1199 building blocks of vision. Nat Rev Neurosci. 15(8):507-19 (2014).
1200 59. Hartveit E, Veruki ML, Zandt BJ. Dendritic Morphology of an Inhibitory Retinal
1201 Interneuron Enables Simultaneous Local and Global Synaptic Integration. J
1202 Neurosci. 42(9):1630-1647 (2022).
1203 60. Liu JH et al. Morphological properties of the axon initial segment-like process of AII
1204 amacrine cells in the rat retina. J Comp Neurol. 529(16):3593-3620 (2021).
1205 61. Branco T, Häusser M. The single dendritic branch as a fundamental functional unit
1206 in the nervous system. Curr Opin Neurobiol. 20:494–502 (2010).
1207 62. Fadjukov J et al. Gap junctions and connexin hemichannels both contribute to the
1208 electrical properties of retinal pigment epithelium. J Gen Physiol. 154(4):
1209 e202112916 (2022).
1210 63. Mills SL, Massey SC. Differential properties of two gap junctional pathways made
1211 by AII amacrine cells. Nature. 377:734-737 (1995).
1212 64. Xia XB, Mills SL. Gap junctional regulatory mechanisms in the AII amacrine cell of
1213 the rabbit retina. Vis Neurosci. 21(5):791-805 (2004).
1214 65. Bloomfield SA, Völgyi B. The diverse functional roles and regulation of neuronal
1215 gap junctions in the retina. Nat Rev Neurosci. 10(7):495-506 (2009).
1216 66. Jacoby J et al. A Self-Regulating Gap Junction Network of Amacrine Cells Controls
1217 Nitric Oxide Release in the Retina. Neuron. 100(5):1149-1162.e5 (2018).

1218 67. Strettoi E, Masri RA & Grünert U. AII amacrine cells in the primate fovea contribute
1219 to photopic vision. Sci Rep. 8, 16429 (2018).
1220 68. Apostolides PF, Trussell LO. Regulation of interneuron excitability by gap junction
1221 coupling with principal cells. Nat Neurosci. 16(12):1764-72 (2013).
1222 69. Song J et al. Motor neurons control locomotor circuit function retrogradely via gap
1223 junctions. Nature. 529(7586):399-402 (2016).
1224 70. Kuo SP, Schwartz GW, Rieke F. Nonlinear Spatiotemporal Integration by Electrical
1225 and Chemical Synapses in the Retina. Neuron 90:320-332 (2016).
1226 71. Manookin MB, Patterson SS, Linehan CM. Neural Mechanisms Mediating Motion
1227 Sensitivity in Parasol Ganglion Cells of the Primate Retina. Neuron. 97(6):1327-
1228 1340.e4 (2018).
1229 72. Pereda AE. Electrical synapses and their functional interactions with chemical
1230 synapses. Nat Rev Neurosci. 15(4):250-63 (2014).
1231 73. Galarreta M, Hestrin S. Spike transmission and synchrony detection in networks of
1232 GABAergic interneurons. Science. 292(5525):2295-9 (2001).
1233 74. Okawa H, Yu W, Matti U et al. Dynamic assembly of ribbon synapses and
1234 circuit maintenance in a vertebrate sensory system. Nat Commun. 10, 2167
1235 (2019).
1236 75. Kuo SP et al. Cone bipolar cell synapses generate transient versus sustained
1237 signals in parallel ON pathways of the mouse retina. eLife. 13:RP98817 (2025).
1238 76. Tetenborg S et al. Differential Distribution of Retinal Ca^{2+}/Calmodulin-Dependent
1239 Kinase II (CaMKII) Isoforms Indicates CaMKII-β and -δ as Specific Elements of
1240 Electrical Synapses Made of Connexin36 (Cx36). Front Mol Neurosci. 10:425
1241 (2017).
1242 77. Tetenborg S et al. Localization of Retinal Ca^{2+}/Calmodulin-Dependent Kinase II-β
1243 (CaMKII-β) at Bipolar Cell Gap Junctions and Cross-Reactivity of Monoclonal Anti-
1244 CaMKII-β Antibody With Connexin36. Front Mol Neurosci. 28; 12:206 (2019).
1245 78. Schmidt TM, Kofuji P. An Isolated Retinal Preparation to Record Light Response
1246 from Genetically Labeled Retinal Ganglion Cells.e2367 (2011).
1247 79. Frederiksen R et al. Rod Photoreceptors Avoid Saturation in Bright Light by the
1248 Movement of the G Protein Transducin. J Neurosci. 41(15):3320-3330 (2021).
1249 80. Khabou H et al. Optogenetic targeting of AII amacrine cells restores retinal
1250 computations performed by the inner retina. Mol Ther Methods Clin Dev.
1251 31:101107 (2023)

1252 81. Meyer A, Yadav SC, Dedek K. Phenotyping of Gap-Junctional Coupling in the
1253 Mouse Retina. Methods Mol Biol. 1753:249-259 (2018).
1254 82. Behrens C et al. Retinal horizontal cells use different synaptic sites for global
1255 feedforward and local feedback signaling. Current Biol.32(3):545-558.e5 (2022).